Stem Cell Reports
Resource
ISSCR
OPEN ACCESS

Network-Based Genomic Analysis of Human Oligodendrocyte Progenitor Differentiation

Suyog U. Pol,[2,3,4] Jessie J. Polanco,[2,4] Richard A. Seidman,[2] Melanie A. O'Bara,[1] Hani J. Shayya,[1] Karen C. Dietz,[1,2] and Fraser J. Sim[1,2,*]
[1]Department of Pharmacology and Toxicology
[2]Neuroscience Program
[3]Department of Biomedical Engineering
School of Medicine and Biomedical Sciences, University at Buffalo, Buffalo NY, USA
[4]Co-first author
*Correspondence: fjsim@buffalo.edu
http://dx.doi.org/10.1016/j.stemcr.2017.07.007

SUMMARY

Impaired human oligodendrocyte progenitor cell (hOPC) differentiation likely contributes to failed remyelination in multiple sclerosis. The characterization of molecular pathways that regulate hOPC differentiation will provide means to induce remyelination. In this study, we determined the gene expression profile of PDGFαR$^+$ hOPCs during initial oligodendrocyte commitment. Weighted gene coexpression network analysis was used to define progenitor and differentiation-specific gene expression modules and functionally important hub genes. These modules were compared with rodent OPC and oligodendrocyte data to determine the extent of species conservation. These analyses identified G-protein β_4 (GNB4), which was associated with hOPC commitment. Lentiviral GNB4 overexpression rapidly induced human oligodendrocyte differentiation. Following xenograft in hypomyelinating *shiverer/rag2* mice, GNB4 overexpression augmented myelin synthesis and the ability of hOPCs to ensheath host axons, establishing GNB4 as functionally important in human myelination. As such, network analysis of hOPC gene expression accurately predicts genes that influence human oligodendrocyte differentiation *in vivo*.

INTRODUCTION

Oligodendrocytes produce myelin that facilitates saltatory conduction in the CNS and provide trophic support to axons (Lee et al., 2012; Morrison et al., 2013). In multiple sclerosis (MS), there is limited capacity for endogenous repair or remyelination (Franklin and Ffrench-Constant, 2008). As failed remyelination in animal models is associated with axonal degeneration (Irvine and Blakemore, 2008), the failure of remyelination in MS likely contributes to progressive disease (Trapp and Nave, 2008). The persistence of undifferentiated oligodendrocyte progenitor cells (OPCs) in MS lesions suggests that interventions that promote OPC commitment and differentiation may improve remyelination (Chang et al., 2000; Kuhlmann et al., 2008). However, it is not clearly understood which signaling cascades are active in human oligodendrocytes and which signals stimulate the early stages of differentiation, regulating the exit from cell cycle and commitment to oligodendrocyte fate.

The molecular processes that underpin oligodendrocyte differentiation in development and following demyelination have been extensively studied (reviewed in Bergles and Richardson, 2015; Wheeler and Fuss, 2016). This has led to the identification of several attractive targets for therapeutic intervention (reviewed in Franklin and Goldman, 2015). Recently, unbiased high-throughput screening methods have identified small molecules and pathways that increase oligodendrocyte differentiation *in vitro* (Deshmukh et al., 2013; Mei et al., 2014; Najm et al., 2015). One limitation of these screens has been the reliance on rodent primary cells. This is important, as the timing and scale of OPC generation are vastly different between humans and rodents and, in some cases, the responses to specific tropic signals differ substantially between species (reviewed in Dietz et al., 2016). We have taken an alternative approach to directly study human primary OPCs by isolation and transcriptomic analysis (Abiraman et al., 2015; Sim et al., 2011; Wang et al., 2013a).

In the current study, we examined the transcriptional processes underlying initial oligodendrocyte commitment of human OPCs (hOPCs) using weighted gene coexpression network analysis (WGCNA) (Zhao et al., 2010). WGCNA enables the identification of gene networks based on a pairwise Pearson correlation of all genes, thus clustering together genes with similar expression patterns. Genes with the greatest contribution or connectivity to these networks often represent functionally important genes and are a commonly referred to as hub genes. WGCNA was previously used to identify cell type-specific hub genes in brain (Miller et al., 2010; Oldham et al., 2008) and functionally relevant genes in glioma (Horvath et al., 2006). A further advantage is that WGCNA permits cross-species analysis to identify both conserved and divergent gene expression between humans and rodents (Miller et al., 2010; Oldham et al., 2006). As such, we also utilized

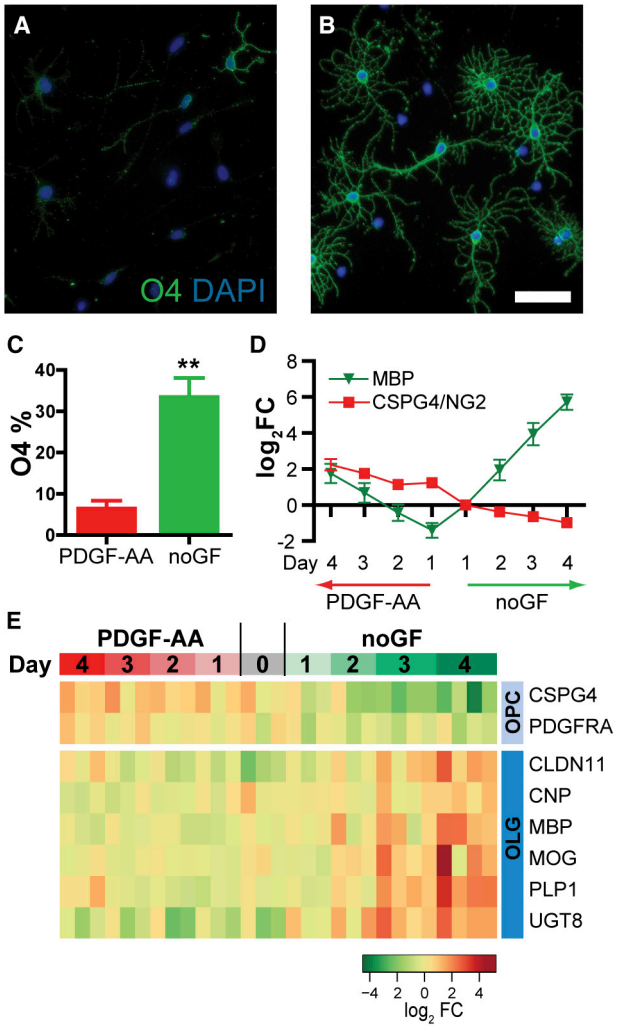

Figure 1. Human Oligodendrocyte Progenitor Cell Differentiation *In Vitro*

(A and B) Human PDGFαR$^+$ OPCs were cultured for 4 days in serum-free medium with PDGF-AA (A) or in the absence of mitogens (no growth factors [noGF]) (B). Cultures were stained for immature oligodendrocyte marker O4 (green). Scale bar, 25 μm.

(C) O4 quantification (mean ± SEM, n = 4 separate human samples). **p < 0.001, t test.

(D) qPCR of *MBP* and *CSPG4* (log_2 fold change relative to day 1 noGF, mean ± SEM, n = 4 human samples).

(E) Heatmap of OPC- and oligodendrocyte-enriched genes.

WGCNA to re-analyze additional datasets from human (Abiraman et al., 2015) and rodent OPCs (Cahoy et al., 2008; Dugas et al., 2006) to define strongly species-conserved gene expression modules associated with oligodendrocyte differentiation. As a proof of concept, we confirmed the expression of several previously uncharacterized OPC- and oligodendrocyte-expressed transcripts and examined their function. We found that G-protein subunit β_4 ($G_{\beta4}$), *GNB4*, was highly upregulated during oligodendrocyte commitment, and that GNB4 overexpression induced oligodendrocyte differentiation of hOPCs. Importantly, $G_{\beta4}$/GNB4 accelerated axonal ensheathment by hOPCs following transplantation. These data suggest that $G_{\beta4}$/GNB4 alters the responsiveness of OPCs to promote differentiation, possibly by altering the effects of other inhibitory G-protein-coupled receptor pathways.

RESULTS

Transcriptional Profiling of Human OPC Differentiation

To determine the transcriptional regulation of hOPC differentiation, we cultured freshly isolated human primary platelet-derived growth factor α receptor (PDGFαR)$^+$ OPCs (Sim et al., 2011) and assessed their differentiation over 4 days *in vitro*. To distinguish between transcriptional changes associated simply with time spent in culture and oligodendrocyte commitment, we treated matched control cultures with PDGF-AA, a known OPC mitogen that delays oligodendrocyte differentiation. hOPCs were fixed on day 4 and assessed for oligodendrocyte differentiation (Figures 1A–1C). As expected, in the absence of PDGF-AA, many cells stained positively for O4 and exhibited a mature branched oligodendrocytic morphology (33.2% ± 4.8%, n = 4 individual tissue samples). A significant fraction of these also expressed myelin basic protein (MBP) (data not shown and Sim et al., 2011). Conversely, in PDGF-AA-containing medium, few cells differentiated as O4$^+$ oligodendrocytes (6.2% ± 4.1%) (Figure 1C).

Total RNA was isolated on each day and qRT-PCR was performed for *MBP* and NG2 (*CSPG4*), a marker of OPCs. Consistent with oligodendrocyte differentiation, MBP mRNA was upregulated more than 300-fold in differentiating conditions (Figure 1D), but was not significantly increased in PDGF-AA-treated cultures (n = 4, one-way ANOVA). Conversely, *CSPG4* mRNA was significantly downregulated in the differentiating conditions and was upregulated by PDGF-AA treatment (n = 4 individual tissue samples, $p < 0.05$, Tukey's post hoc test) (Figure 1D).

To characterize the transcriptional responses attendant with human oligodendrocyte differentiation, we performed microarray analysis. RNA was purified from matched cultures derived from four individual patient brain samples. We first examined markers of OPCs and oligodendrocyte differentiation. hOPCs cultured in differentiating conditions exhibited a time-dependent progressive increase in expression of myelin protein genes, including *CLDN11*, *MBP*, *MOG*, and *PLP1*, and a corresponding decrease in *PDGFRA* and *CSPG4* (Figure 1E). These effects were effectively blocked by PDGF-AA,

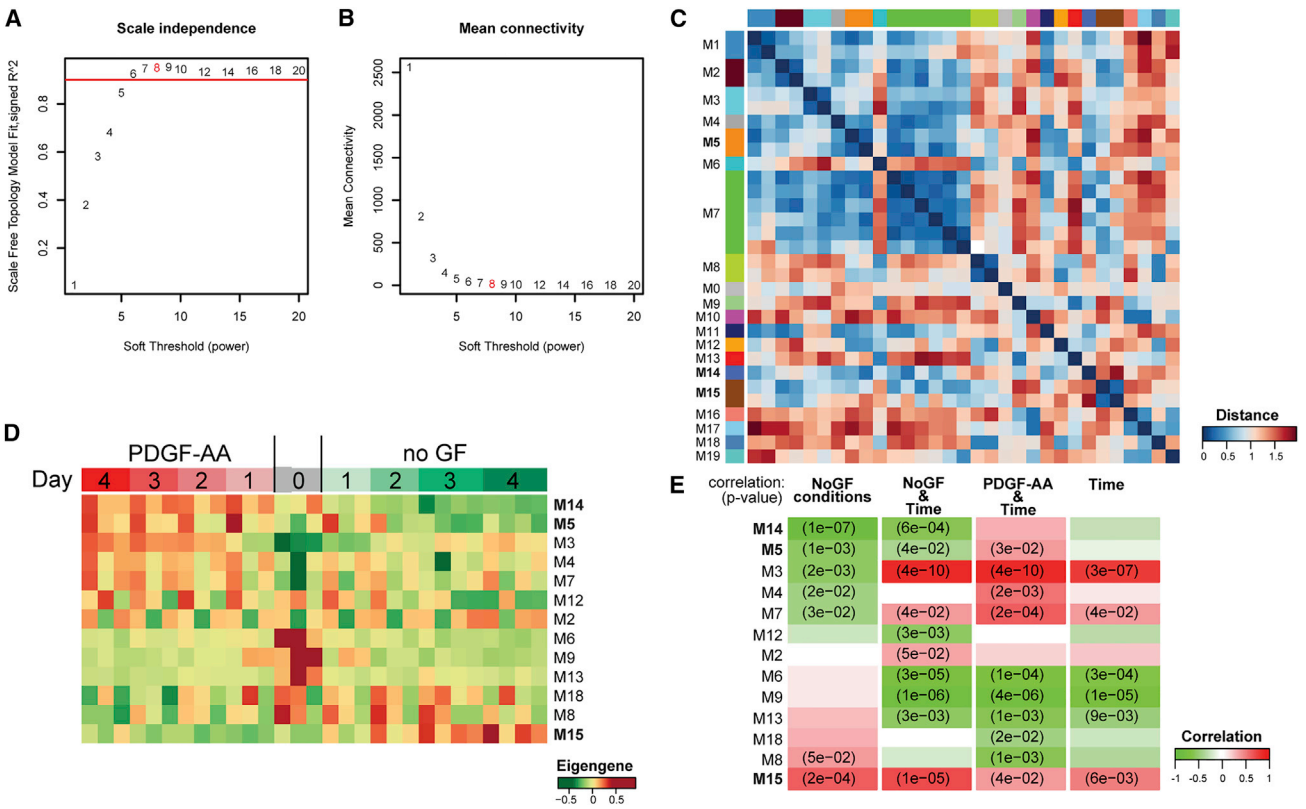

Figure 2. Weighted Gene Coexpression Network Analysis of hOPC Differentiation

(A and B) Analysis of network topology to determine soft-thresholding power. (A) Fit of power-transformed gene-pairwise Pearson correlation to scale-free topology as a function of soft threshold. (B) Mean network connectivity as a function of soft threshold. Soft-thresholding power of 8 was selected to maximize the model fit.

(C) Heatmap of Pearson correlation between eigengenes of WGCNA modules.

(D) Expression profiles of merged module eigengene illustrate distinct expression patterns in final network.

(E) Correlation of module eigengenes with experimental variables: time, culture condition (PDGF-AA, noGF), and their interaction.

allowing us to discriminate between time- and differentiation-dependent effects.

Weighted Gene Coexpression Network Analysis of Human OPC Differentiation

To take full advantage of time as a continuous parameter and to systematically analyze the gene expression profile of hOPC differentiation in an unsupervised fashion, we applied WGCNA. WGCNA is a network analysis-based technique that utilizes the extent of gene-gene coregulation to determine functionally relevant modules or sets of genes (Zhao et al., 2010). In brief, pairwise Pearson correlations were power-transformed to calculate adjacency values, which penalize weakly correlated genes. The power was selected to ensure that the resulting gene network conformed to a biologically relevant scale-free topology (Figure 2A) and maximized the connectedness of genes within the network, i.e., it maximized the net adjacency values (Figure 2B). Topological overlap, which quantifies the similarity in adjacency values associated with two genes, was used in unsupervised hierarchical gene clustering. As such, each gene was grouped into modules containing other highly coregulated and connected genes. Analysis of each module's first principal component, referred to as its eigengene, revealed several highly related modules (Figure 2C). As described previously (Oldham et al., 2008), we merged highly related modules to generate a final network composed of 20 distinct modules.

We examined the expression profile of each module's eigengene, which is considered representative of the gene expression profiles contained in that module (Horvath and Dong, 2008). Several module eigengene profiles were significantly correlated with experimental parameters, such as media conditions and time *in vitro* (Figure 2E). For example, M3 was highly correlated with time ($r = 0.79$, $p = 1.3 \times 10^{-7}$) but was negatively correlated with culture

in differentiating conditions (no growth factors [noGF], $r = -0.55$, $p = 0.002$). Using this approach, we focused on modules with eigengenes that correlated with the pro-differentiating conditions (noGF) and time (Figures 2D and 2E). Of note, modules M14 ($r = 0.81$, $p = 1 \times 10^{-7}$) and M5 ($r = 0.57$, $p = 0.001$) were strongly correlated with progenitor growth conditions (PDGF-AA) but not dependent on time, consistent with maintenance of OPC fate. M15 represented the only module showing upregulation and positive correlation with differentiating conditions ($r = 0.63$, $p = 2.0 \times 10^{-4}$).

WGCNA Identifies Conserved Modules Expressed during Human and Rodent OPC Differentiation

WGCNA provides a platform-independent approach to compare gene expression across experiments and species (Miller et al., 2010; Oldham et al., 2006). We performed WGCNA on three additional independent datasets that examined OPC transcriptional profiles. We reanalyzed (1) rat primary OPCs undergoing differentiation *in vitro* (Dugas et al., 2006); (2) primary mouse isolated OPCs and oligodendrocytes (Cahoy et al., 2008), and (3) primary human isolated OPCs and early oligodendrocytes (Abiraman et al., 2015). Following matched approaches for normalization and summarization, human homologs were found and annotated in the rodent datasets and WGCNA performed. We identified 19 modules in Dugas, 7 modules in Cahoy, and 10 modules in Abiraman datasets (Figure S1).

Following cross-species annotation, the number of homologous genes shared between individual modules (M1–M15) and each of the modules identified in the other three datasets were calculated in a pairwise fashion. The significance of theses module-module relationships was determined by calculation of hypergeometric probabilities for each pair (Table S1). Intriguingly, only two modules identified in the analysis of hOPC differentiation *in vitro* were preserved across the other three datasets (false discovery rate [FDR]-corrected hypergeometric test) (Figure 3). Several modules were found to have significant overlap with only one dataset. For example, M3D, which we found to be regulated by time *in vitro* in hOPCs, was similarly regulated in rat OPCs *in vitro* (Figure S2), suggesting that this module represents an artifact of gene regulation governed by cell culture. M2C, which was only conserved in hOPC differentiation and the Cahoy mouse dataset (FDR-corrected hypergeometric test, $p = 0.002$), was instead characterized by genes expressed in cultured astrocytes (Figure S2). In contrast, both M5 and M15, which were preserved across all datasets, were found to have highly consistent eigengene profiles associated with high expression observed in OPCs and oligodendrocytes, respectively. This suggests that M5 and M15 comprise functionally important and conserved modules in the regulation of OPC commitment and differentiation.

Conserved OPC and Oligodendrocyte Modules Were Functionally Distinct

To determine the principal constituents of modules M5 and M15, we performed pathway analysis by determining the relative over-representation of individual genes within each module using gene ontology (GO) (Table S2). Module M5 and its homologs across the other datasets were enriched for GO terms associated with RNA synthesis including ribosomal subunit biogenesis and assembly. We defined hub genes, which have been shown to act as potential regulators of the entire module (Johnson et al., 2009; Oldham et al., 2008), using intra-module connectivity, i.e., the summation of all Pearson gene-gene correlations. Shared among the M5 hub genes (Figure 4A) and its homologs, we noted ribosomal proteins S5/S9/S15 and heterogeneous nuclear ribonucleoprotein A/B (*HNRNPAB*), which is involved in mRNA splicing and pre-mRNA processing and regulates gene expression in neurogenic progenitors (Lein et al., 2007), and may act to delay oligodendrocyte differentiation (Sinnamon et al., 2012). Both human networks contained several genes involved in mitochondrial electron transport (M5 and M5A, $p < 0.001$). We also noted *PTPRZ1* in both M5 and M5D; *PTPRZ1* is involved in hOPC self-renewal (McClain et al., 2012) and differentiation (Sim et al., 2006). Together, this suggested active roles for transcription and metabolism for module M5 that are conserved in human and rodent OPCs.

Consistent with increased expression during differentiation across the four datasets, M15 was significantly enriched for genes involved in myelination (M15, $p = 0.001$; M15C, $p < 0.001$), and oligodendrocyte (M15C, $p = 0.003$) and glial (M15A, $p = 0.001$) differentiation. Importantly, the essential oligodendrocyte transcription factor, *MYRF*, was identified among the hub genes in M15 (human differentiation) (Figure 4B), M15C (mouse), and M15A (human FACS). (Note: the microarray used in the Cahoy dataset did not contain probes against MYRF). Likewise, several other known oligodendrocyte genes were identified in M15 and its homologs. Therefore, M15 was characterized as an oligodendrocyte differentiation module, which was conserved across species.

Identification of Regulators of Human OPC Commitment and Differentiation

To provide proof of concept that WGCNA identified functionally relevant genes, we examined module M15 for genes with no known function in oligodendrocytes (Table 1). We focused on genes with differential upregulation in differentiated oligodendrocytes and those that were preserved across M15 homologs. The most highly

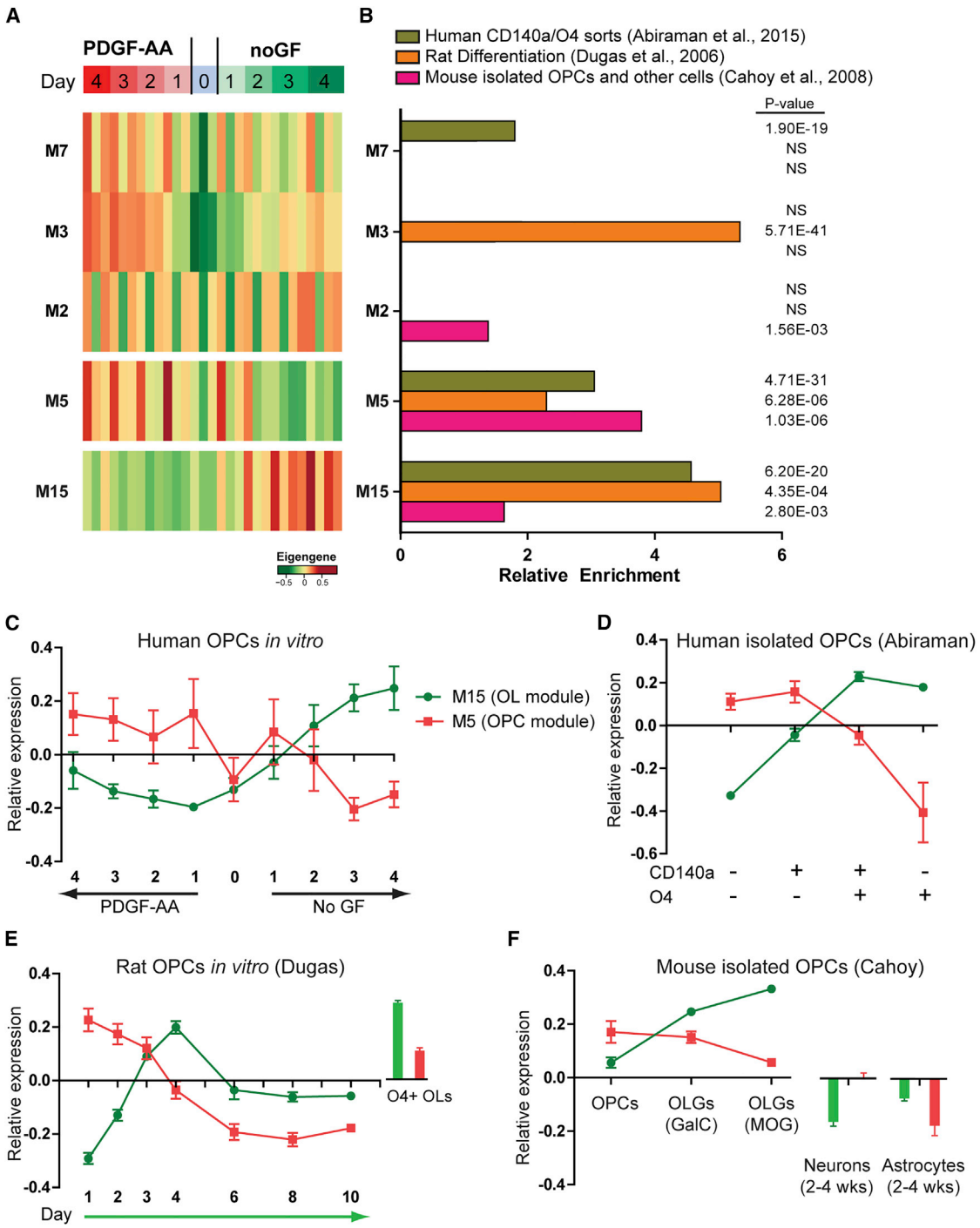

Figure 3. Conservation of OPC and Oligodendrocyte WGCNA Modules between Species

WGCNA was performed on rat oligodendrocytes (OLGs) (Dugas et al., 2006), isolated mouse OPCs/OLGs (Cahoy et al., 2008), and isolated hOPCs (Abiraman et al., 2015). Following module overlap analysis between these datasets, only five modules exhibited substantial and significant overlap ($p < 0.05$, FDR-corrected hypergeometric test).

(A) Heatmap of eigengene expression for the five modules.

(B–F) Relative enrichment of shared genes in each matching module (compared with random list) and corresponding hypergeometric test p value. Eigengene expression profiles of cross-species-conserved modules M15 and M5 in differentiating hOPCs (C), human isolated OPCs (D), rat differentiating OPCs (E), and isolated mouse OPCs/OLGs (F). Mean ± SEM.

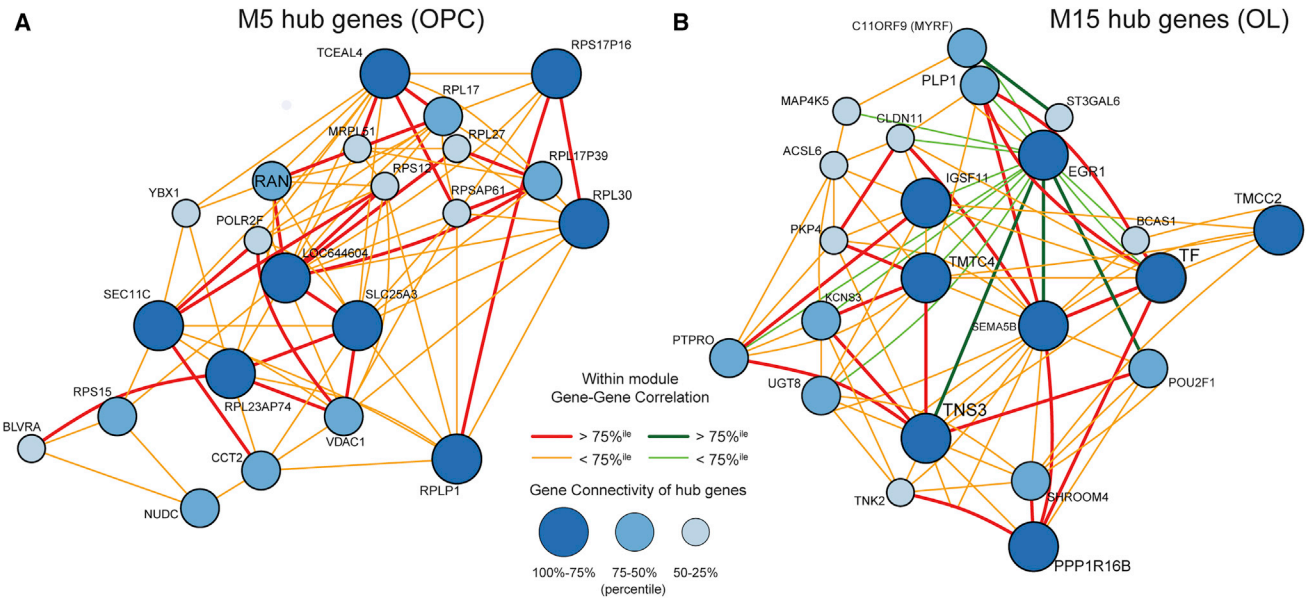

Figure 4. Hub Genes of OPC and OLG Modules

Species-conserved OPC and oligodendrocyte differentiation-specific modules M5 (A) and M15 (B) were further examined to identify hub genes, which were expected to exert the largest influence on module constituents. The top 30 genes were selected based on the sum of intra-module connectivity between genes. The node size for each hub gene represents the relative hubness, and connection color indicates both the direction and degree of correlation with other hub genes.

upregulated was breast cancer amplified sequence 1, *BCAS1*, which was increased more than 50-fold in differentiating hOPCs and preserved in both M15 and M15C. Additionally, *BCAS1* was significantly enriched in human O4$^+$ oligodendrocytes (Abiraman et al., 2015) as well as in epiblast-derived oligodendrocytes (Najm et al., 2011). We confirmed that *BCAS1* was significantly regulated using qPCR (Figure S3A) ($n = 4$ individual fetal samples, repeated-measures ANOVA, $F(7,21) = 53.1$, $p < 0.0001$). Consistent with the microarray data, *BCAS1* was strongly and progressively upregulated with time in differentiating conditions (Tukey's post hoc test, $p < 0.001$ between each day). *PPP1R16B*, protein phosphatase 1 regulatory subunit 16B, was preserved only in the hOPC FACS dataset (M15A), but was also highly expressed by mouse MOG$^+$ oligodendrocytes (Cahoy et al., 2008). qPCR confirmed upregulation of *PPP1R16B* in differentiation conditions (Figure 5A), as well as strong upregulation with time (Tukey's post hoc $p < 0.001$). Finally, we identified guanine nucleotide-binding protein subunit $G_{\beta 4}$ (*GNB4*) as the only M15 upregulated transcript whose expression was also preserved in M15D and M15A modules, but was also increased in mouse oligodendrocytes (Cahoy et al., 2008) and differentiating mouse Oli-Neu OPCs (Gobert et al., 2009). Consistent with the WGCNA predictions, *GNB4* was significantly upregulated progressively each day during OPC commitment (Figure 5A) ($p < 0.05$).

To determine whether the expression of these genes might be sufficient to drive oligodendrocyte differentiation from hOPCs, we overexpressed *BCAS1*, *PPP1R16B*, and *GNB4* in hOPCs. For *PPP1R16B* and *GNB4*, hOPCs were infected with lentivirus and cultured for 4 days in the absence of PDGF-AA. We initially assessed the extent of O4$^+$ oligodendrocyte differentiation. Interestingly, both *GNB4* and *PPR1R16B* significantly increased the percentage of O4$^+$ oligodendrocytes compared with mCherry controls ($n = 4$ fetal samples; 1-way ANOVA, $F(2,8) = 18.4$, Dunnett's post hoc test versus mCherry, $p < 0.01$) (Figures 5D and 5E). GNB4-infected cells developed into oligodendrocytes with highly complex and branched morphologies, often extending O4$^+$ processes that contacted and extended along neighboring cells. In contrast, *BCAS1* overexpression did not influence oligodendrocyte differentiation (Figures S3B and S3C).

The increased proportion of O4$^+$ oligodendrocytes following PPP1R16B or GNB4 overexpression could be due to multiple effects on OPC fate. Therefore, we examined effects on cell number, lineage commitment, and proliferation. The increase in O4 percentage was not accompanied by changes in overall live cell number between groups (one-way ANOVA, $F(2,8) = 0.2$, $p = 0.82$) (Figure S4A).

We further analyzed the effects of GNB4 overexpression on OPC lineage commitment and proliferation. GNB4 overexpression did not alter the percentage of OLIG2$^+$ cells

Table 1. Differentially Expressed Genes in Module M15

Symbol	NCBI Entrez ID	Description	M15 Connectivity (Rank)	Day 4 versus Day 0 (No GF)		Preserved in		
				Log_2 FC	q Value	M15D	M15C	M15A
BCAS1	8537	breast carcinoma amplified sequence 1	17.0 (22)	5.80	3.29×10^{-6}		X	
PPP1R16B	26051	protein phosphatase 1, subunit 16B	21.0 (6)	2.95	1.42×10^{-3}			X
GNB4	59345	G protein β_4	7.7 (119)	2.43	2.09×10^{-4}	X		X
HEXDC	284004	hexosaminidase D	6.1 (159)	2.08	2.88×10^{-3}			X
MAN2A2	4122	mannosidase α class 2A2	5.8 (168)	1.93	2.28×10^{-3}			
POU2F1	5451	POU class 2 homeobox 1	18.8 (12)	1.78	2.04×10^{-3}			
DUSP22	100134291	similar to MAPK phosphatase x	7.8 (118)	1.72	7.92×10^{-4}			
NPHP3	27031	nephronophthisis 3	1.9 (368)	1.58	1.56×10^{-3}			

Previously undescribed members of oligodendrocyte differentiation module M15 were identified that exhibited differential expression during oligodendrocyte differentiation, day 4 versus day 0 in differentiating conditions (log_2 FC > 1, q value < 0.01). "X" indicates significant overlap between modules by FDR-corrected hypergeometric testing.

(65% ± 11% versus 56% ± 8% mCherry; p = 0.55; n = 4 fetal samples) (Figures S4B–S4G). As an increase in $O4^+$ cells could be caused by reduced OPC proliferation, we bromodeoxyuridine (BrdU)-pulsed matched cultures. The percentage of $BrdU^+$ proliferating cells in *GNB4*-infected cells did not differ from mCherry cells (63% ± 12% versus 59% ± 13% mCherry; t test p = 0.42; n = 4 fetal samples). In contrast, BCAS1 overexpression substantially reduced BrdU incorporation (Figures S3D and S3E). Together, these data suggested that GNB4 and PPP1R16B overexpression were sufficient to drive OPC commitment to oligodendrocyte fate.

As the pro-differentiation effect of GNB4 overexpression was so pronounced, we sought to determine whether *GNB4* expression was required for differentiation. Using three distinct and specific small interfering RNAi (siRNAi) sequences, we transfected proliferating hOPCs. Individual siRNA transfection was sufficient to knock down GNB4 mRNA by more than 90%, with the combined transfection reducing expression by >95% (98.2% ± 0.1% versus scrambled control, p < 0.0001, n = 3 fetal samples). Surprisingly, *GNB4* knockdown of combined or individual siRNA sequences resulted in substantial cell death at 48 hr after transfection, characterized by process retraction, surface detachment, and reduced live cell number compared with matched cultures transfected with control non-targeting siRNA (Figure S5). Importantly, this effect was specific to *GNB4,* as other siRNAs did not influence cell survival (data not shown). Cell death following *GNB4* knockdown was observed in OPCs maintained under both proliferating and pro-differentiation conditions. As such, these results indicate that $G_{\beta 4}$ expression is necessary for the survival of hOPCs.

GNB4/$G_{\beta 4}$ Overexpression Attenuates Inhibitory GPCR Signaling in Human OPCs

G-protein-coupled receptors (GPCRs) are key regulators of OPC differentiation in development and disease. For example, muscarinic receptor signaling inhibits oligodendrocyte differentiation and acts to delay myelin repair by transplanted hOPCs and remyelination in rodent models (Abiraman et al., 2015; Deshmukh et al., 2013; Mei et al., 2014). While all five β subunits were expressed in OPCs and differentiating oligodendrocytes (Figure S6), only *GNB4* mRNA was upregulated during OPC differentiation and was enriched in OPCs relative to other neural cell types (Abiraman et al., 2015; Cahoy et al., 2008; Dugas et al., 2006). Individual Gβ subunits are known to influence specific GPCR effector signaling pathways (Khan et al., 2013). As GPCR muscarinic agonists block hOPC differentiation, we sought to establish whether GNB4 overexpression could influence muscarinic agonist-induced calcium oscillations mediated by the G_q-coupled M_1 or M_3 receptor. Using a lentiviral GCaMP6s to express a calcium-sensitive fluorescence reporter, we observed that the muscarinic agonist oxotremorine-M induced calcium waves in a dose-dependent manner with a typical duration of >4 min and frequency of 30–50 mHz. GNB4 overexpression did not alter the amplitude or frequency of calcium waves (Figure 6A) or the proportion of responding hOPCs ($logEC_{50}$ = −5.9 ± 0.2 versus −6.5 ± 0.3 for mCherry and GNB4, respectively; Figure S7) compared with mCherry control hOPCs. Thus, GNB4 likely does not influence muscarinic receptor-mediated inhibition of oligodendrocyte differentiation.

To more broadly assess the mechanisms by which GNB4 regulates signaling in hOPCs, we determined the effects of GNB4 overexpression on several common

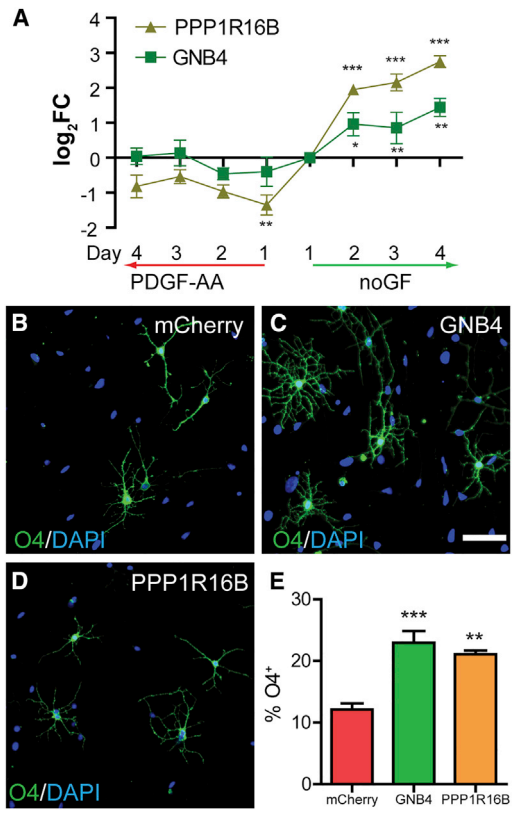

Figure 5. Overexpression of PPP16R1B and GNB4 Induces hOPC Differentiation *In Vitro*

(A) qPCR of *PPP16R1B* and *GNB4* in proliferating (PDGF-AA) or differentiating (noGF) conditions (mean ± SEM $\log_2$ fold change relative to day-1 conditions, n = 4 patient samples, Tukey's post test versus day-1 noGF conditions).

(B–D) hOPCs were infected with lentiviruses overexpressing GNB4 (C), PPP1R16B (D), or mCherry (control) (B). The extent of $O4^+$ oligodendrocyte differentiation was assessed at 4 days post infection.

(E) Both PPP16R1B and GNB4 overexpression resulted in a significant increase in the proportion of $O4^+$ cells (mean ± SEM, n = 4, repeated measures 1-way ANOVA, Dunnett's post hoc test).

*p < 0.05, **p < 0.01, ***p < 0.001, post test. Scale bar, 50 μm.

signaling pathways using a panel of lentiviral luciferase reporters. GNB4 overexpression did not induce either cyclic AMP/protein kinase A (CREB) or protein kinase C/Ca^{2+} (NFAT) signaling, which is consistent with lack of effect on muscarinic signaling (Figure 6B). In serum-free conditions without mitogens, basal signaling was only detected in ERK (ELK-1/SRF) and JNK (AP-1) pathways (Figure 6B). Interestingly, both pathways were strongly activated following lentiviral GNB4 overexpression. While JNK signaling has not been associated with OPC differentiation, ERK1/2 activation is known to promote oligodendrocyte differentiation and myelin synthesis (Fyffe-Maricich et al., 2011; Ishii et al., 2012) and, therefore, may contribute to the observed effects of GNB4/$G_{\beta4}$ expression on hOPC differentiation.

GNB4/$G_{\beta4}$ Promotes Human Oligodendrocyte Differentiation and Axon Ensheathment

To further establish a functional role of $G_{\beta4}$ in hOPC differentiation, we utilized the *shiverer/rag2* model of hypomyelination that models stem cell-mediated myelin repair and enables assessments of human myelination *in vivo* (Abiraman et al., 2015; Wang et al., 2014). Following infection with either GNB4- or mCherry-expressing lentivirus, 10^5 hOPCs were transplanted directly into the corpus callosum of postnatal day 2 *shiverer/rag2* pups. Recipient animals were euthanized at 8 weeks, at which time very few hOPCs have typically undergone differentiation into MBP-expressing oligodendrocytes (Abiraman et al., 2015; Sim et al., 2011). Human nuclear antigen (hNA)-positive cells were found in the corpus callosum at 8 weeks with a similar density and distribution in both groups (911 ± 275 versus 902 ± 121 hNA^+ cells for mCherry and GNB4, respectively; n = 4–7 mice) (Figures 7A and 7B).

To determine the effect of GNB4 overexpression on oligodendrocyte maturation, we assessed MBP immunohistochemistry which is absent in *shiverer* mice. Strikingly, animals transplanted with GNB4-expressing hOPCs exhibited a greater than 3-fold increase in MBP staining within the corpus callosum (p = 0.003) (Figures 7A–7C). Consistent with improved myelination by GNB4-expressing transplanted cells, the density of ensheathed axons increased from 40.5 ± 5.1 fibers/mm by mCherry control cells to 71.8 ± 9.8 fibers/mm by GNB4-expressing cells, representing a >75% increase in axonal ensheathment (p = 0.028; n = 4) (Figures 7D–7F). Thus, GNB4-expressing hOPCs more rapidly synthesized MBP and ensheathed host axons, consistent with accelerated donor-derived myelin synthesis.

Surprisingly, the observed increase in myelination was not accompanied by an increase in the proportion of hOPCs undergoing oligodendrocyte differentiation, as the percentage of $CC1^+$ oligodendrocytes was not altered (Figures 7G and 7J). The increase in extent of MBP expression and axon ensheathment was, therefore, not due to a substantial increase in oligodendrocyte number, but rather an increased rate of oligodendrocyte maturation. In addition, we observed that GNB4 expression increased the proportion of human glial fibrillary protein $(GFAP)^+$ astrocytes (p < 0.05; n = 4–7) (Figures 7H and 7K). Finally, GNB4 expression did not alter the proportion of Ki-67^+ proliferating cells compared with mCherry control cells (Figures 7I and 7L). Taken together, these data establish that $G_{\beta4}$ expression differentially regulates hOPC fate *in vitro* and *in vivo* and, importantly, GNB4/$G_{\beta4}$ was sufficient to

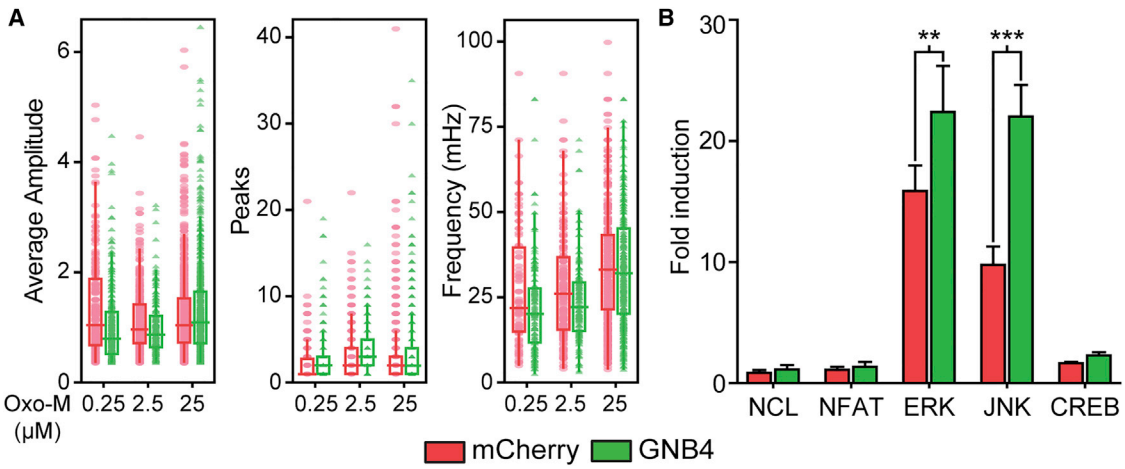

Figure 6. GNB4/$G_{\beta 4}$ Overexpression Induces MAPK Signaling

Fetal PDGFαR$^+$ hOPCs were cultured and infected with intracellular Ca^{2+} reporter GCaMP6s. Following GNB4 or mCherry overexpression, time-lapse microscopy of Ca^{2+} response after Oxo-M treatment was recorded and analyzed.

(A) Individual responsive cell Ca^{2+} measurements for average spike amplitude (left), total number of peaks (center), and frequency (right), along with their box plot. GNB4 overexpression did not significantly change Ca^{2+} response ($p > 0.05$, $n > 90$ cells per condition, two-way ANOVA with Tukey's HSD post test, $n = 3$).

(B) hOPC signaling was measured using luciferase-based reporter after infection with GNB4 or mCherry lentivirus. Activity is reported as fold change in luminescence compared with negative control. $^{**}p < 0.01$, $^{***}p < 0.001$ ($n = 3$), two-way ANOVA with Bonferroni post test.

substantially improve the production of myelin proteins and axonal ensheathment by hOPCs *in vivo*.

DISCUSSION

The transcriptional processes involved in the initial stages oligodendrocyte differentiation have been examined in detail using rodent primary and stem cell-derived progenitors (Dugas et al., 2006; Gobert et al., 2009; Najm et al., 2011; Zhang et al., 2014). However, the extent to which these pathways and mechanisms are conserved during human development is less understood. We previously compared the transcriptional profile of freshly isolated human cells to their rodent homologs, with hOPCs isolated from both fetal (Abiraman et al., 2015; Sim et al., 2011) and adult (Sim et al., 2006, 2009) human brain. The aim of this study was to establish the extent of conservation between human and rodent programs of initial oligodendrocyte differentiation using a network-based analytic approach. Using a longitudinal experimental design, we could analyze the gene expression of matched OPCs isolated from individual patient samples and predict the function of genes previously undescribed in hOPC differentiation.

Rather than profile the transcriptome of pluripotent stem cell-derived OPCs, which may not accurately represent the phenotype of endogenous progenitors, we isolated primary OPCs from fetal human brain using PDGFαR-based cell sorting at a developmental stage during which OPCs undergo massive expansion in the forebrain (Sim et al., 2011). Similar to primary rat OPCs (Dugas et al., 2006), following the initiation of oligodendrocyte differentiation we observed an exponential increase in MBP mRNA expression in hOPCs occurring over the first 4 days. Indeed, our transcriptional analysis captured an expression profile of early myelin-enriched genes very similar to that defined previously (Dugas et al., 2006), and as such was suitable for comparisons between species. Furthermore, we incorporated PDGF-AA treatment to distinguish between genes whose expression was regulated by the process of oligodendrocyte differentiation and not simply a consequence of time spent *in vitro*.

Using this experimental approach and WGCNA, we identified several modules containing genes with highly related functions. Five modules were associated with progenitor maintenance and function, while only a single module was associated with differentiation. Interestingly, each of the OPC upregulated eigengene modules had distinct functional annotations. For example, M3 was associated with DNA replication and cell-cycle processes and M14 with proteasome function and G_1 cycle checkpoint regulation. The species-conserved module M5 was associated with ribosome function and translation, and was highly enriched in MYC target genes (Enrichr/ChEA analysis) (Kuleshov et al., 2016; Lachmann et al., 2010).

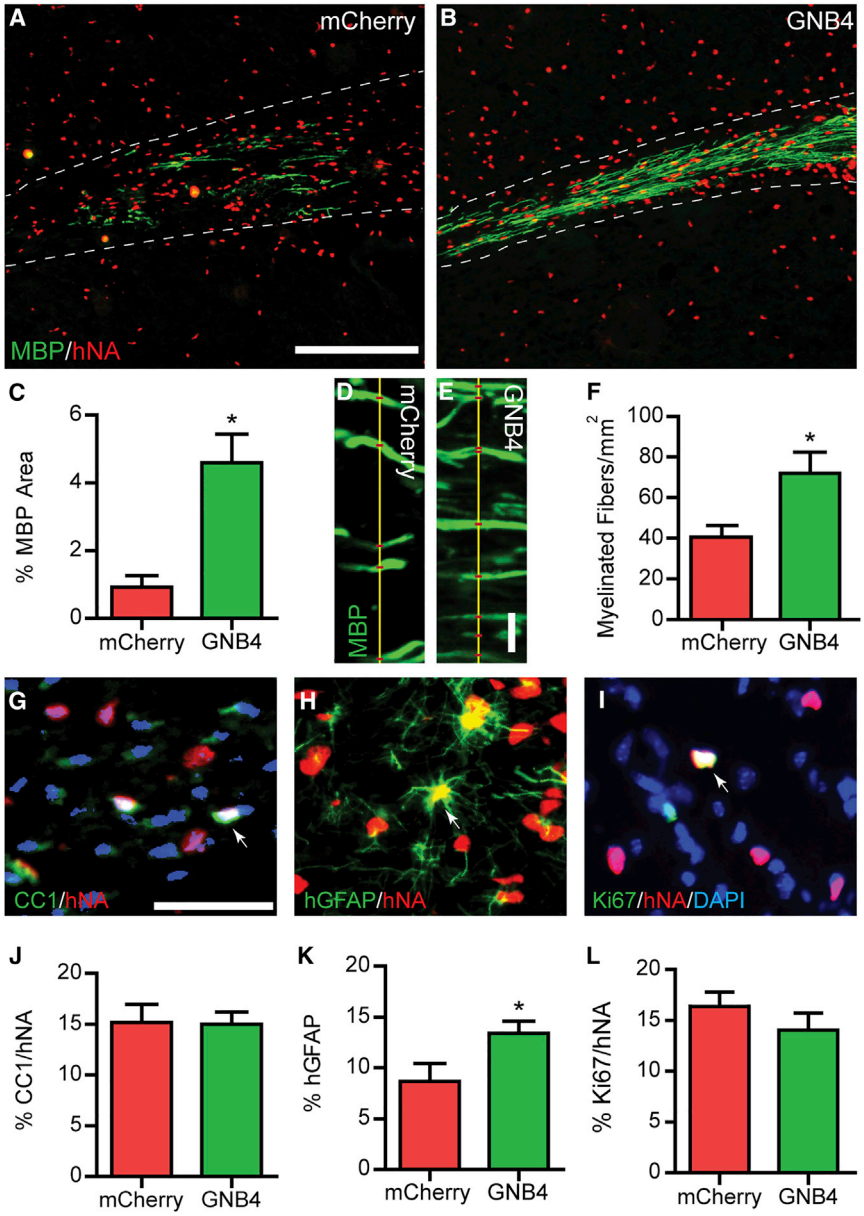

Figure 7. GNB4/$G_{\beta 4}$ Overexpression Enhances Human Myelination by Transplanted hOPCs

GNB4 or mCherry overexpressing hOPCs were transplanted into the corpus callosum of 2- to 3-day *shiverer/rag2* mice and euthanized at 8 weeks to assess engraftment and myelination.

(A and B) Immunostaining for human nuclear antigen (hNA) and MBP to assess engraftment and oligodendrocyte differentiation (corpus callosum outlined by dotted lines).

(C) Quantification of MBP area as a proportion of corpus callosum (mean ± SEM, n = 3–6 mice).

(D and E) Confocal microscopy of MBP^+ ensheathed axons.

(F) Density of myelinated axons was quantified within engrafted regions (mean ± SEM, n = 3–4).

(G–L) Cell fate was assessed by immunofluorescence for $CC1^+hNA^+$ human oligodendrocytes (G), $hGFAP^+hNA^+$ human astrocytes (H), and $Ki\text{-}67^+hNA^+$ dividing human cells (I). Arrows indicate double-positive human cells in each panel. The proportion is quantified in (J) to (L). GNB4 did not significantly effect oligodendrocyte maturation (J) or proliferation (L) among transplanted cells, but increased the proportion of differentiated astrocytes (K), compared with mCherry controls.

*$p < 0.05$, n = 3–6 mice per group, unpaired t test. Scale bars, 100 μm (A; applies also to B), 10 μm (E; applies also to D), and 25 μm (G; applies also to H and I).

As such, WGCNA segregates genes associated with biochemically distinct biological processes that were associated with progenitor maintenance.

The observation that only a single WGCNA module was associated with differentiation suggests that the initiation of differentiation involves a largely unitary coordinated gene expression program. Among the M15 hub genes, we found known transcription factors that regulate positive (*MYRF*, *SOX8*) and negative (*EGR1*, *EGR2*, *ID4*) aspects of oligodendrocyte differentiation. Intriguingly, an analysis of M15 hub genes by Enrichr/ChEA chromatin immunoprecipitation enrichment analysis identified M15 gene expression as likely regulated by a combination of well-characterized oligodendrocyte transcription factors (*OLIG2*, Brg1/*SMARCA4*), as well as *MITF*, *WT1*, and *SMAD4*. This is consistent with the known transcription factor hierarchy in which OLIG2/SMARCA4 regulates SOX and MYRF factors to initiate differentiation (Yu et al., 2013), and BMP/SMAD regulation of *OLIG2*/*ID4* to conversely inhibit differentiation (Samanta, 2004). In addition, this suggested a previously undescribed role for MITF or other members of the TFE family in oligodendrocyte differentiation. It is noteworthy that these factors physically interact with one another (Laurette et al., 2015; Wang et al., 2016) and thereby could compete to generate a bistable transcriptional switch.

To better determine whether WGCNA could predict functionally relevant genes, we selected candidate genes based on their expression patterns in human and rodent systems and M15 module membership. We selected three candidates for functional validation: *BCAS1*, *PPP1R16B*, and *GNB4*. While *BCAS1* had no effect on differentiation, both *PP1R16B* and *GNB4* induce precocious $O4^+$ oligodendrocyte differentiation when overexpressed *in vitro*. BCAS1 overexpression reduced hOPC proliferation but did not affect oligodendrocyte differentiation. Interestingly, BCAS1 null mice were recently described and display a very mild hypomyelinating phenotype in the CNS, suggesting a non-essential role in oligodendrocyte development (Ishimoto et al., 2017).

PPP1R16B overexpression increased hOPC-oligodendrocyte differentiation. PPP1R16B is a regulatory subunit of protein phosphatase 1 (PP1) that may act to target the catalytic subunit of PP1 to specific membrane-associated proteins (Ito et al., 2004). The complex of PP1 with regulatory subunits provides target specificity and compartmentalization within the cell (Cohen, 2002). In the CNS, *PPP1R16B* mRNA is highly enriched in early differentiating human and mouse oligodendrocytes and localized to spinal cord white matter in postnatal day 4 spinal cord (Allen Brain Atlas). As PPP1R16B is regulated by cyclic AMP/protein kinase A in endothelial cells and has been shown to block PTEN function (Obeidat et al., 2014), it is possible that PP1R16B may act to potentiate phosphatidylinositol 3-kinase/Akt signaling in newly generated oligodendrocytes and thereby promote the maturation of progenitors to oligodendrocytes (Flores et al., 2008).

Heterotrimeric G proteins composed of Gα and Gβγ subunits are key signaling transducers that are activated by GPCRs and modulate a variety of intracellular signaling cascades. While Gα subunits have clearly defined roles, the role of specific Gβγ dimers and individual Gβ subunits is less clear (Khan et al., 2013). $G_{\beta4}$/GNB4 is one of five Gβ proteins in humans, sharing greatest homology with $G_{\beta1}$. While all except GNB3 mRNA were expressed in oligodendrocyte lineage cells, only *GNB4* mRNA was upregulated during oligodendrocyte differentiation and was enriched compared with neurons and astrocytes. *GNB1/2* mRNAs were quantitatively more abundant in hOPCs than *GNB4*, suggesting that upregulation of $G_{\beta4}$ may interfere with signal transduction mediated by $G\beta_{1/2}$ as well as promote specific $G_{\beta4}$-coupled signaling.

We found that overexpression of GNB4 increased oligodendrocyte formation *in vitro* and potentiated oligodendrocyte maturation and axonal ensheathment following transplantation. This suggests that GNB4 expression is rate limiting during oligodendrocyte differentiation and that increased expression could be employed to promote the differentiation of OPCs. Intriguingly, genomic mutations in GNB4 have been associated with dominant intermediate Charcot-Marie-Tooth disease (Soong et al., 2013). As $G_{\beta4}$ protein is localized to peripheral nervous system myelin, this suggests a critical role for GNB4 in Schwann cells and peripheral myelination. In hOPCs, *GNB4* siRNAi induced rapid cell death, indicating that this subunit is also required for OPC survival. The observed effects of GNB4 overexpression on hOPC-mediated myelin repair suggest that GNB4 accelerates differentiation *in vitro* and promotes myelin maturation *in vivo*. After transplantation, while we did not observe an effect of GNB4 on $CC1^+$ oligodendrocyte density, a far greater number of myelinated internodes was produced. As such, driving GNB4 expression in OPCs derived from pluripotent stem cells might represent a useful strategy to potentiate the formation of oligodendrocytes and accelerate the otherwise protracted protocols that are necessary (Douvaras et al., 2014; Wang et al., 2013b). Indeed, strategies to increase GNB4 expression might be envisaged to augment transplant-mediated myelin repair without affecting overall cell density or reducing the progenitor pool.

In conclusion, we have defined the gene expression profile of hOPCs undergoing oligodendrocyte differentiation. By using WGCNA on several datasets obtained in human, mouse, and rat primary cells, we identified gene expression modules containing highly coordinated genes that were expressed across species. This approach identified GNB4/$G_{\beta4}$ as a previously undescribed gene involved in OPC differentiation and as a target to improve myelin repair by transplanted progenitors. This database includes several other important candidates likely to regulate important aspects of human oligodendrocyte commitment and differentiation (www.FindDb.org). We anticipate that these data will provide a valuable resource for analyzing oligodendrocyte differentiation in rodents and as a point of reference for comparing primary and pluripotent stem cell-derived progenitors and their differentiated progeny.

EXPERIMENTAL PROCEDURES

Preparation of Human PDGFαR$^+$ OPCs

Fetal brain samples (18–22 weeks gestational age) were obtained from patients who consented to tissue use under protocols approved by the SUNY at Buffalo HSIRB. Tissue was dissociated and PDGFαR$^+$ hOPCs prepared as previously described (Sim et al., 2011) (see Supplemental Experimental Procedures).

Immunocytochemistry, Real-Time RT-PCR, Calcium Imaging, and Luciferase Analysis

hOPC culture and immunocytochemistry were performed as described by Abiraman et al. (2015). Antibody details are provided in Table S3. For assessment of gene expression, RNA was extracted

(Omega Bio-Tek) and real-time RT-PCR performed (see Table S4 for list of primers). Calcium imaging in response to muscarinic agonist was performed following infection with GCaMP6s-expressing lentivirus using a motorized epifluorescence microscope (Olympus) and analyzed using R software (complete description in Supplemental Experimental Procedures). Luciferase reporter assays were performed according to the manufacturer's instructions following infection of hOPCs with Cignal Lentiviral reporters (Qiagen) and quantified using Bright-Glo (Promega).

Gene Expression and WGCNA

Gene expression analysis was performed using Illumina whole-genome arrays and analyzed using R/Bioconductor (see Supplemental Experimental Procedures for complete details). WGCNA was performed on each dataset (Langfelder and Horvath, 2008). Following identification of human homologs, species-conserved modules were identified by hypergeometric testing and corrected by false discovery rate.

Viral Expression and siRNA

GNB4, PPP1R16B, and GCaMP6s overexpression lentiviruses were generated by subcloning into pTRIP-EF1α (a gift from A. Benraiss, University of Rochester). Retroviral BCAS1-IRES-GFP and control viral plasmids were provided by M. Petryniak (Oregon Health & Science University). GNB4 siRNA (Thermo Fisher Scientific) was transfected as per manufacturer's instructions (100 μM).

Transplantation

All experiments using *shiverer/rag2* mice were performed according to protocols approved by the University at Buffalo Institutional Animal Care and Use Committee. As previously described (Wang et al., 2014), 10^5 hOPCs were implanted into *shiverer/rag2* neonatal corpus callosum and euthanized at 8 weeks post implantation. Confocal and wide-field immunofluorescence (Supplemental Experimental Procedures and Table S3) was performed to assess hOPC engraftment, cell fate, and axonal ensheathment.

Statistical Analyses

All statistical analyses were performed using GraphPad Prism (San Diego, CA). Data were compared by Student's t test, one-way ANOVA, or two-way ANOVA, where appropriate; significance was considered at $p < 0.05$.

SUPPLEMENTAL INFORMATION

Supplemental Information includes Supplemental Experimental Procedures, seven figures, and four tables and can be found with this article online at http://dx.doi.org/10.1016/j.stemcr.2017.07.007.

AUTHOR CONTRIBUTIONS

S.U.P., J.J.P., R.A.S., M.A.O., H.J.S., K.C.D., and F.J.S. performed experiments and analyzed data. S.U.P., J.J.P., R.A.S., and F.J.S. provided intellectual contributions. S.U.P., J.J.P., K.C.D., and F.J.S. wrote the paper.

ACKNOWLEDGMENTS

This work was supported by the NIH (NCATS, UL1TR001412), the National Multiple Sclerosis Society (RG 5505-A-2), the Kalec Multiple Sclerosis Foundation, the Change MS Foundation, the Skarlow Memorial Trust, and the Empire State Stem Cell Fund through New York State Department of Health Contract (C028108). We thank Dr. J. Conroy of Roswell Park Cancer Institute for assistance with Illumina Beadarray techniques. The microarray profiling was supported by grants from the NIH/National Cancer Institute, P30 CA016056 (RPCI Cancer Center support grant). We acknowledge the assistance of the Confocal Microscope and Flow Cytometry Facility in the School of Medicine and Biomedical Sciences, University at Buffalo. We thank Dr. Magdalena A. Petryniak, Department of Pediatrics, Oregon Health & Science University, for assistance with BCAS1 retrovirus. We thank David Bratton and Aberlee J. Milliron for technical assistance.

Received: January 3, 2017
Revised: July 6, 2017
Accepted: July 7, 2017
Published: August 8, 2017

REFERENCES

Abiraman, K., Pol, S.U., O'Bara, M.A., Chen, G.D., Khaku, Z.M., Wang, J., Thorn, D., Vedia, B.H., Ekwegbalu, E.C., Li, J.X., et al. (2015). Anti-muscarinic adjunct therapy accelerates functional human oligodendrocyte repair. J. Neurosci. *35*, 3676–3688.

Bergles, D.E., and Richardson, W.D. (2015). Oligodendrocyte development and plasticity. Cold Spring Harb. Perspect. Biol. *8*, a020453.

Cahoy, J.D., Emery, B., Kaushal, A., Foo, L.C., Zamanian, J.L., Christopherson, K.S., Xing, Y., Lubischer, J.L., Krieg, P.A., Krupenko, S.A., et al. (2008). A transcriptome database for astrocytes, neurons, and oligodendrocytes: a new resource for understanding brain development and function. J. Neurosci. *28*, 264–278.

Chang, A., Nishiyama, A., Peterson, J., Prineas, J., and Trapp, B.D. (2000). NG2-positive oligodendrocyte progenitor cells in adult human brain and multiple sclerosis lesions. J. Neurosci. *20*, 6404–6412.

Cohen, P.T. (2002). Protein phosphatase 1—targeted in many directions. J. Cell Sci. *115*, 241–256.

Deshmukh, V.A., Tardif, V., Lyssiotis, C.A., Green, C.C., Kerman, B., Kim, H.J., Padmanabhan, K., Swoboda, J.G., Ahmad, I., Kondo, T., et al. (2013). A regenerative approach to the treatment of multiple sclerosis. Nature *502*, 327–332.

Dietz, K.C., Polanco, J.J., Pol, S.U., and Sim, F.J. (2016). Targeting human oligodendrocyte progenitors for myelin repair. Exp. Neurol. *283*, 489–500.

Douvaras, P., Wang, J., Zimmer, M., Hanchuk, S., O'Bara, M.A., Sadiq, S., Sim, F.J., Goldman, J., and Fossati, V. (2014). Efficient generation of myelinating oligodendrocytes from primary progressive multiple sclerosis patients by induced pluripotent stem cells. Stem Cell Reports *3*, 250–259.

Dugas, J.C., Tai, Y.C., Speed, T.P., Ngai, J., and Barres, B.A. (2006). Functional genomic analysis of oligodendrocyte differentiation. J. Neurosci. *26*, 10967–10983.

Flores, A.I., Narayanan, S.P., Morse, E.N., Shick, H.E., Yin, X., Kidd, G., Avila, R.L., Kirschner, D.A., and Macklin, W.B. (2008). Constitutively active Akt induces enhanced myelination in the CNS. J. Neurosci. *28*, 7174–7183.

Franklin, R.J., and Ffrench-Constant, C. (2008). Remyelination in the CNS: from biology to therapy. Nat. Rev. Neurosci. *9*, 839–855.

Franklin, R.J., and Goldman, S.A. (2015). Glia disease and repair-remyelination. Cold Spring Harb. Perspect. Biol. *7*, a020594.

Fyffe-Maricich, S.L., Karlo, J.C., Landreth, G.E., and Miller, R.H. (2011). The ERK2 mitogen-activated protein kinase regulates the timing of oligodendrocyte differentiation. J. Neurosci. *31*, 843–850.

Gobert, R.P., Joubert, L., Curchod, M.L., Salvat, C., Foucault, I., Jorand-Lebrun, C., Lamarine, M., Peixoto, H., Vignaud, C., Fremaux, C., et al. (2009). Convergent functional genomics of oligodendrocyte differentiation identifies multiple autoinhibitory signaling circuits. Mol. Cell. Biol. *29*, 1538–1553.

Horvath, S., and Dong, J. (2008). Geometric interpretation of gene coexpression network analysis. PLoS Comput. Biol. *4*, e1000117.

Horvath, S., Zhang, B., Carlson, M., Lu, K.V., Zhu, S., Felciano, R.M., Laurance, M.F., Zhao, W., Qi, S., Chen, Z., et al. (2006). Analysis of oncogenic signaling networks in glioblastoma identifies ASPM as a molecular target. Proc. Natl. Acad. Sci. USA *103*, 17402–17407.

Irvine, K.A., and Blakemore, W.F. (2008). Remyelination protects axons from demyelination-associated axon degeneration. Brain *131*, 1464–1477.

Ishii, A., Fyffe-Maricich, S.L., Furusho, M., Miller, R.H., and Bansal, R. (2012). ERK1/ERK2 MAPK signaling is required to increase myelin thickness independent of oligodendrocyte differentiation and initiation of myelination. J. Neurosci. *32*, 8855–8864.

Ishimoto, T., Ninomiya, K., Inoue, R., Koike, M., Uchiyama, Y., and Mori, H. (2017). Mice lacking BCAS1, a novel myelin-associated protein, display hypomyelination, schizophrenia-like abnormal behaviors, and upregulation of inflammatory genes in the brain. Glia *65*, 727–739.

Ito, M., Nakano, T., Erdodi, F., and Hartshorne, D.J. (2004). Myosin phosphatase: structure, regulation and function. Mol. Cell. Biochem. *259*, 197–209.

Johnson, M.B., Kawasawa, Y.I., Mason, C.E., Krsnik, Z., Coppola, G., Bogdanovic, D., Geschwind, D.H., Mane, S.M., State, M.W., and Sestan, N. (2009). Functional and evolutionary insights into human brain development through global transcriptome analysis. Neuron *62*, 494–509.

Khan, S.M., Sleno, R., Gora, S., Zylbergold, P., Laverdure, J.P., Labbe, J.C., Miller, G.J., and Hebert, T.E. (2013). The expanding roles of Gbetagamma subunits in G protein-coupled receptor signaling and drug action. Pharmacol. Rev. *65*, 545–577.

Kuhlmann, T., Miron, V., Cui, Q., Wegner, C., Antel, J., and Bruck, W. (2008). Differentiation block of oligodendroglial progenitor cells as a cause for remyelination failure in chronic multiple sclerosis. Brain *131*, 1749–1758.

Kuleshov, M.V., Jones, M.R., Rouillard, A.D., Fernandez, N.F., Duan, Q., Wang, Z., Koplev, S., Jenkins, S.L., Jagodnik, K.M., Lachmann, A., et al. (2016). Enrichr: a comprehensive gene set enrichment analysis web server 2016 update. Nucleic Acids Res. *44*, W90–W97.

Lachmann, A., Xu, H., Krishnan, J., Berger, S.I., Mazloom, A.R., and Ma'ayan, A. (2010). ChEA: transcription factor regulation inferred from integrating genome-wide ChIP-X experiments. Bioinformatics *26*, 2438–2444.

Langfelder, P., and Horvath, S. (2008). WGCNA: an R package for weighted correlation network analysis. BMC Bioinformatics *9*, 559.

Laurette, P., Strub, T., Koludrovic, D., Keime, C., Le Gras, S., Seberg, H., Van Otterloo, E., Imrichova, H., Siddaway, R., Aerts, S., et al. (2015). Transcription factor MITF and remodeller BRG1 define chromatin organisation at regulatory elements in melanoma cells. Elife *4*, e06857.

Lee, Y., Morrison, B.M., Li, Y., Lengacher, S., Farah, M.H., Hoffman, P.N., Liu, Y., Tsingalia, A., Jin, L., Zhang, P.W., et al. (2012). Oligodendroglia metabolically support axons and contribute to neurodegeneration. Nature *487*, 443–448.

Lein, E.S., Hawrylycz, M.J., Ao, N., Ayres, M., Bensinger, A., Bernard, A., Boe, A.F., Boguski, M.S., Brockway, K.S., Byrnes, E.J., et al. (2007). Genome-wide atlas of gene expression in the adult mouse brain. Nature *445*, 168–176.

McClain, C.R., Sim, F.J., and Goldman, S.A. (2012). Pleiotrophin suppression of receptor protein tyrosine phosphatase-beta/zeta maintains the self-renewal competence of fetal human oligodendrocyte progenitor cells. J. Neurosci. *32*, 15066–15075.

Mei, F., Fancy, S.P., Shen, Y.A., Niu, J., Zhao, C., Presley, B., Miao, E., Lee, S., Mayoral, S.R., Redmond, S.A., et al. (2014). Micropillar arrays as a high-throughput screening platform for therapeutics in multiple sclerosis. Nat. Med. *20*, 954–960.

Miller, J.A., Horvath, S., and Geschwind, D.H. (2010). Divergence of human and mouse brain transcriptome highlights Alzheimer disease pathways. Proc. Natl. Acad. Sci. USA *107*, 12698–12703.

Morrison, B.M., Lee, Y., and Rothstein, J.D. (2013). Oligodendroglia: metabolic supporters of axons. Trends Cell Biol. *23*, 644–651.

Najm, F.J., Zaremba, A., Caprariello, A.V., Nayak, S., Freundt, E.C., Scacheri, P.C., Miller, R.H., and Tesar, P.J. (2011). Rapid and robust generation of functional oligodendrocyte progenitor cells from epiblast stem cells. Nat. Methods *8*, 957–962.

Najm, F.J., Madhavan, M., Zaremba, A., Shick, E., Karl, R.T., Factor, D.C., Miller, T.E., Nevin, Z.S., Kantor, C., Sargent, A., et al. (2015). Drug-based modulation of endogenous stem cells promotes functional remyelination in vivo. Nature *522*, 216–220.

Obeidat, M., Li, L., and Ballermann, B.J. (2014). TIMAP promotes angiogenesis by suppressing PTEN-mediated Akt inhibition in human glomerular endothelial cells. Am. J. Physiol. Ren. Physiol. *307*, F623–F633.

Oldham, M.C., Horvath, S., and Geschwind, D.H. (2006). Conservation and evolution of gene coexpression networks in human and chimpanzee brains. Proc. Natl. Acad. Sci. USA *103*, 17973–17978.

Oldham, M.C., Konopka, G., Iwamoto, K., Langfelder, P., Kato, T., Horvath, S., and Geschwind, D.H. (2008). Functional organization of the transcriptome in human brain. Nat. Neurosci. *11*, 1271–1282.

Samanta, J. (2004). Interactions between ID and OLIG proteins mediate the inhibitory effects of BMP4 on oligodendroglial differentiation. Development *131*, 4131–4142.

Sim, F.J., Lang, J.K., Waldau, B., Roy, N.S., Schwartz, T.E., Pilcher, W.H., Chandross, K.J., Natesan, S., Merrill, J.E., and Goldman, S.A. (2006). Complementary patterns of gene expression by human oligodendrocyte progenitors and their environment predict determinants of progenitor maintenance and differentiation. Ann. Neurol. *59*, 763–779.

Sim, F.J., Windrem, M.S., and Goldman, S.A. (2009). Fate determination of adult human glial progenitor cells. Neuron Glia Biol. *5*, 45–55.

Sim, F.J., McClain, C.R., Schanz, S.J., Protack, T.L., Windrem, M.S., and Goldman, S.A. (2011). CD140a identifies a population of highly myelinogenic, migration-competent and efficiently engrafting human oligodendrocyte progenitor cells. Nat. Biotechnol. *29*, 934–941.

Sinnamon, J.R., Waddell, C.B., Nik, S., Chen, E.I., and Czaplinski, K. (2012). Hnrpab regulates neural development and neuron cell survival after glutamate stimulation. RNA *18*, 704–719.

Soong, B.W., Huang, Y.H., Tsai, P.C., Huang, C.C., Pan, H.C., Lu, Y.C., Chien, H.J., Liu, T.T., Chang, M.H., Lin, K.P., et al. (2013). Exome sequencing identifies GNB4 mutations as a cause of dominant intermediate Charcot-Marie-Tooth disease. Am. J. Hum. Genet. *92*, 422–430.

Trapp, B.D., and Nave, K.A. (2008). Multiple sclerosis: an immune or neurodegenerative disorder? Annu. Rev. Neurosci. *31*, 247–269.

Wang, J., O'Bara, M.A., Pol, S.U., and Sim, F.J. (2013a). CD133/CD140a-based isolation of distinct human multipotent neural progenitor cells and oligodendrocyte progenitor cells. Stem Cells Dev. *22*, 2121–2131.

Wang, S., Bates, J., Li, X., Schanz, S., Chandler-Militello, D., Levine, C., Maherali, N., Studer, L., Hochedlinger, K., Windrem, M., et al. (2013b). Human iPSC-derived oligodendrocyte progenitor cells can myelinate and rescue a mouse model of congenital hypomyelination. Cell Stem Cell *12*, 252–264.

Wang, J., Pol, S.U., Haberman, A.K., Wang, C., O'Bara, M.A., and Sim, F.J. (2014). Transcription factor induction of human oligodendrocyte progenitor fate and differentiation. Proc. Natl. Acad. Sci. USA *111*, E2885–E2894.

Wang, C., Zhao, L., Su, Q., Fan, X., Wang, Y., Gao, S., Wang, H., Chen, H., Chan, C.B., and Liu, Z. (2016). Phosphorylation of MITF by AKT affects its downstream targets and causes TP53-dependent cell senescence. Int. J. Biochem. Cell Biol. *80*, 132–142.

Wheeler, N.A., and Fuss, B. (2016). Extracellular cues influencing oligodendrocyte differentiation and (re)myelination. Exp. Neurol. *283*, 512–530.

Yu, Y., Chen, Y., Kim, B., Wang, H., Zhao, C., He, X., Liu, L., Liu, W., Wu, L.M., Mao, M., et al. (2013). Olig2 targets chromatin remodelers to enhancers to initiate oligodendrocyte differentiation. Cell *152*, 248–261.

Zhang, Y., Chen, K., Sloan, S.A., Bennett, M.L., Scholze, A.R., O'Keeffe, S., Phatnani, H.P., Guarnieri, P., Caneda, C., Ruderisch, N., et al. (2014). An RNA-sequencing transcriptome and splicing database of glia, neurons, and vascular cells of the cerebral cortex. J. Neurosci. *34*, 11929–11947.

Zhao, W., Langfelder, P., Fuller, T., Dong, J., Li, A., and Hovarth, S. (2010). Weighted gene coexpression network analysis: state of the art. J. Biopharm. Stat. *20*, 281–300.

Stem Cell Reports, Volume *9*

Supplemental Information

Network-Based Genomic Analysis of Human Oligodendrocyte Progenitor Differentiation

Suyog U. Pol, Jessie J. Polanco, Richard A. Seidman, Melanie A. O'Bara, Hani J. Shayya, Karen C. Dietz, and Fraser J. Sim

Dugas; Rat OPC differentiation

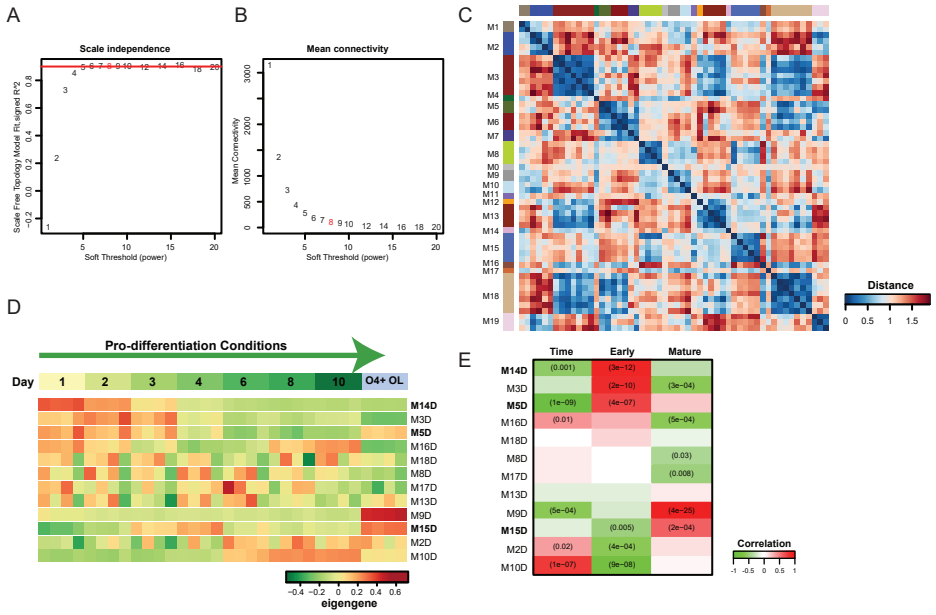

Cahoy; Mouse isolated neural populations

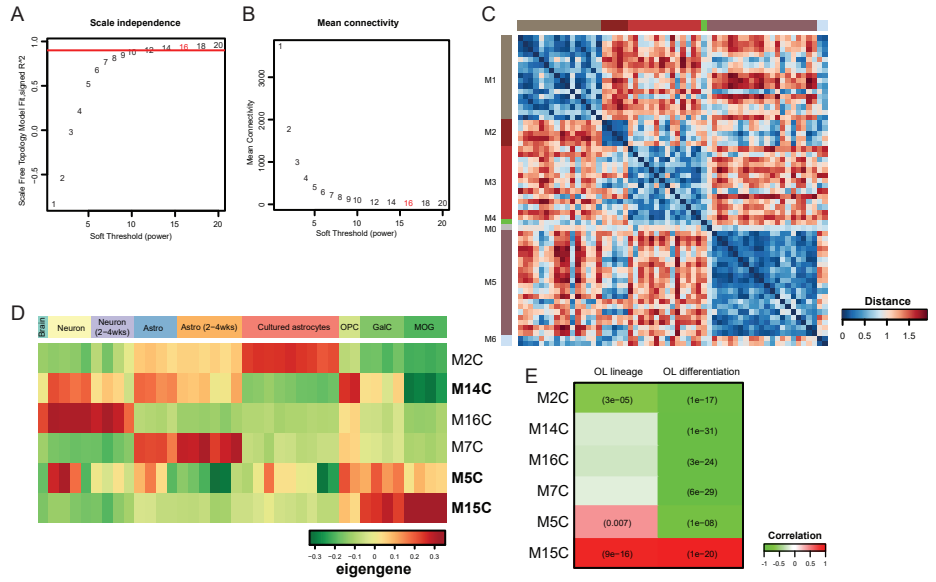

Abiraman; Human isolated OPCs

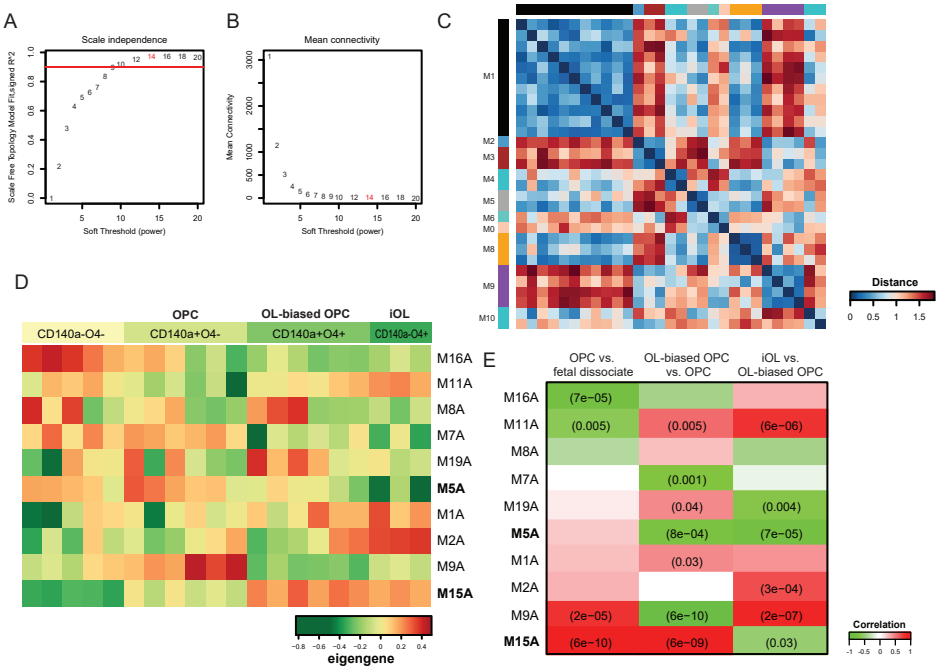

Figure S2

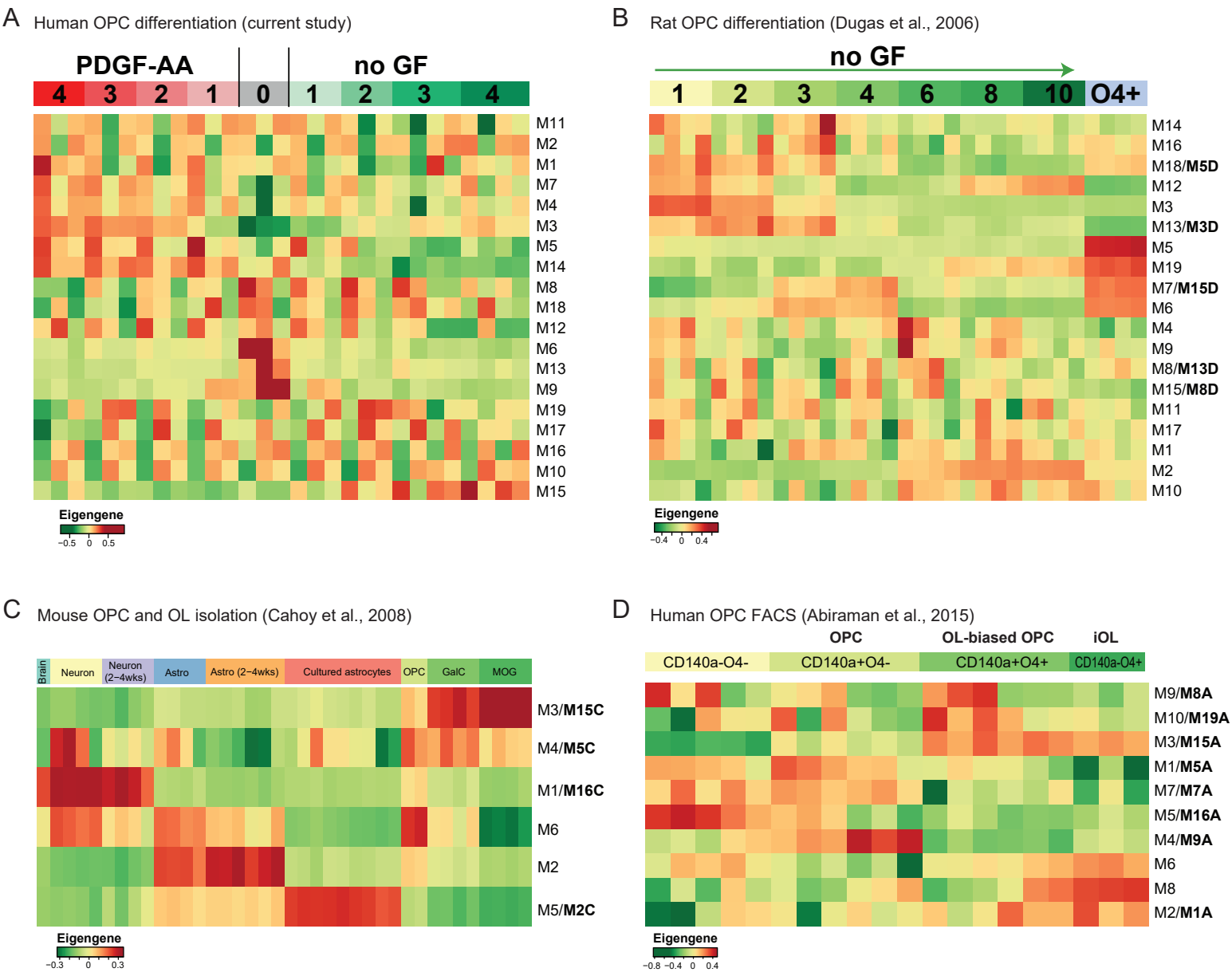
A
Human OPC differentiation (current study)
PDGF-AA
no GF
4 3 2 1 0 1 2 3 4
M11 M2 M1 M7 M4 M3 M5 M14 M8 M18 M12 M6 M13 M9 M19 M17 M16 M10 M15
Eigengene
−0.5 0 0.5
B
Rat OPC differentiation (Dugas et al., 2006)
no GF
1 2 3 4 6 8 10 O4+
M14 M16 M18/M5D M12 M3 M13/M3D M5 M19 M7/M15D M6 M4 M9 M8/M13D M15/M8D M11 M17 M1 M2 M10
Eigengene
−0.4 0 0.4
C
Mouse OPC and OL isolation (Cahoy et al., 2008)
Brain
Neuron
Neuron (2−4wks)
Astro
Astro (2−4wks)
Cultured astrocytes
OPC
GalC
MOG
M3/M15C M4/M5C M1/M16C M6 M2 M5/M2C
Eigengene
−0.3 0 0.3
D
Human OPC FACS (Abiraman et al., 2015)
OPC
OL-biased OPC
iOL
CD140a-O4-
CD140a+O4-
CD140a+O4+
CD140a-O4+
M9/M8A M10/M19A M3/M15A M1/M5A M7/M7A M5/M16A M4/M9A M6 M8 M2/M1A
Eigengene
−0.8 −0.4 0 0.4

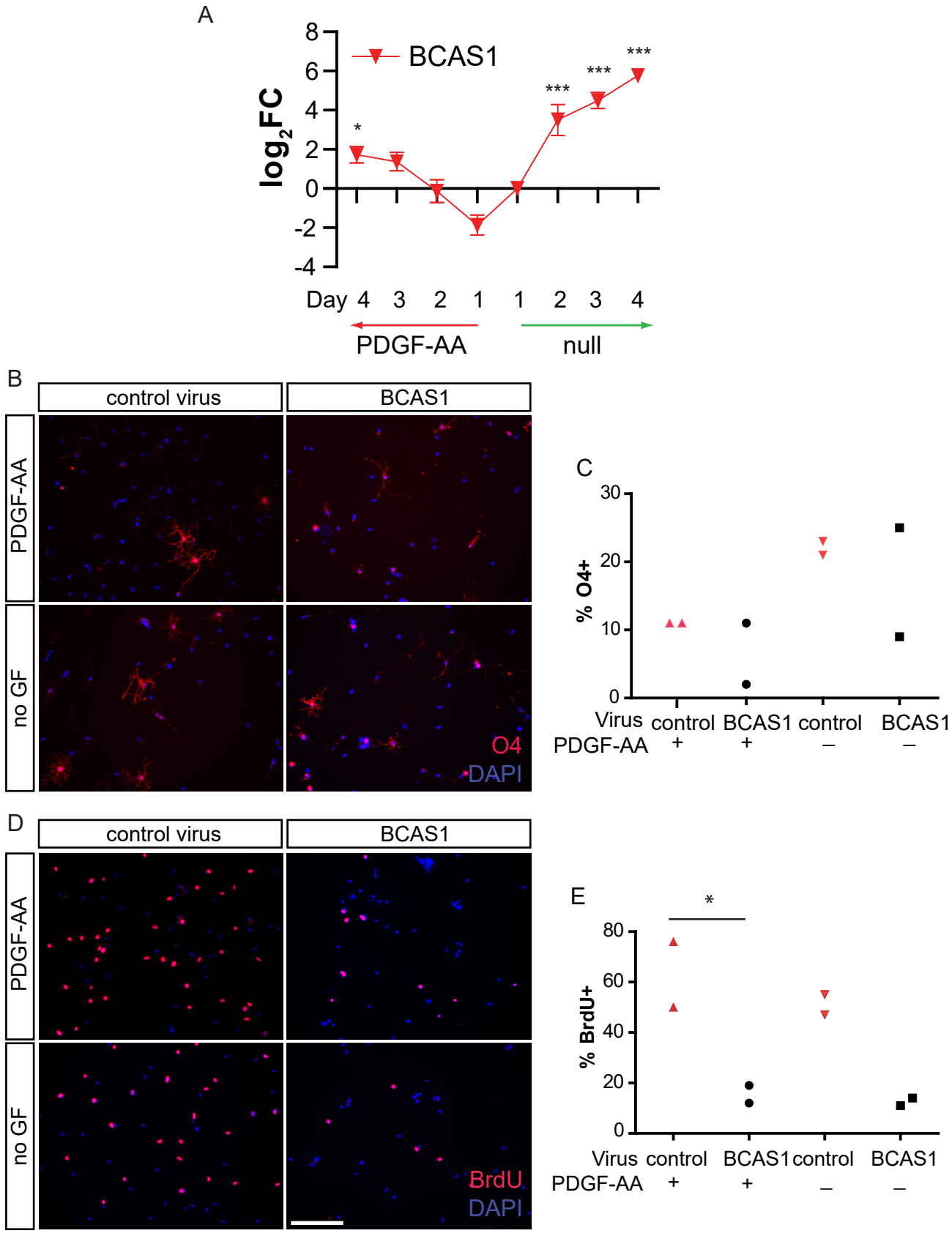
A
BCAS1
log2FC
8
6
4
2
0
-2
-4
*
***
***
***
Day 4 3 2 1 1 2 3 4
PDGF-AA
null
B
control virus
BCAS1
PDGF-AA
no GF
O4
DAPI
C
% O4+
30
20
10
0
Virus control BCAS1 control BCAS1
PDGF-AA + + – –
D
control virus
BCAS1
PDGF-AA
no GF
BrdU
DAPI
E
*
% BrdU+
80
60
40
20
0
Virus control BCAS1 control BCAS1
PDGF-AA + + – –

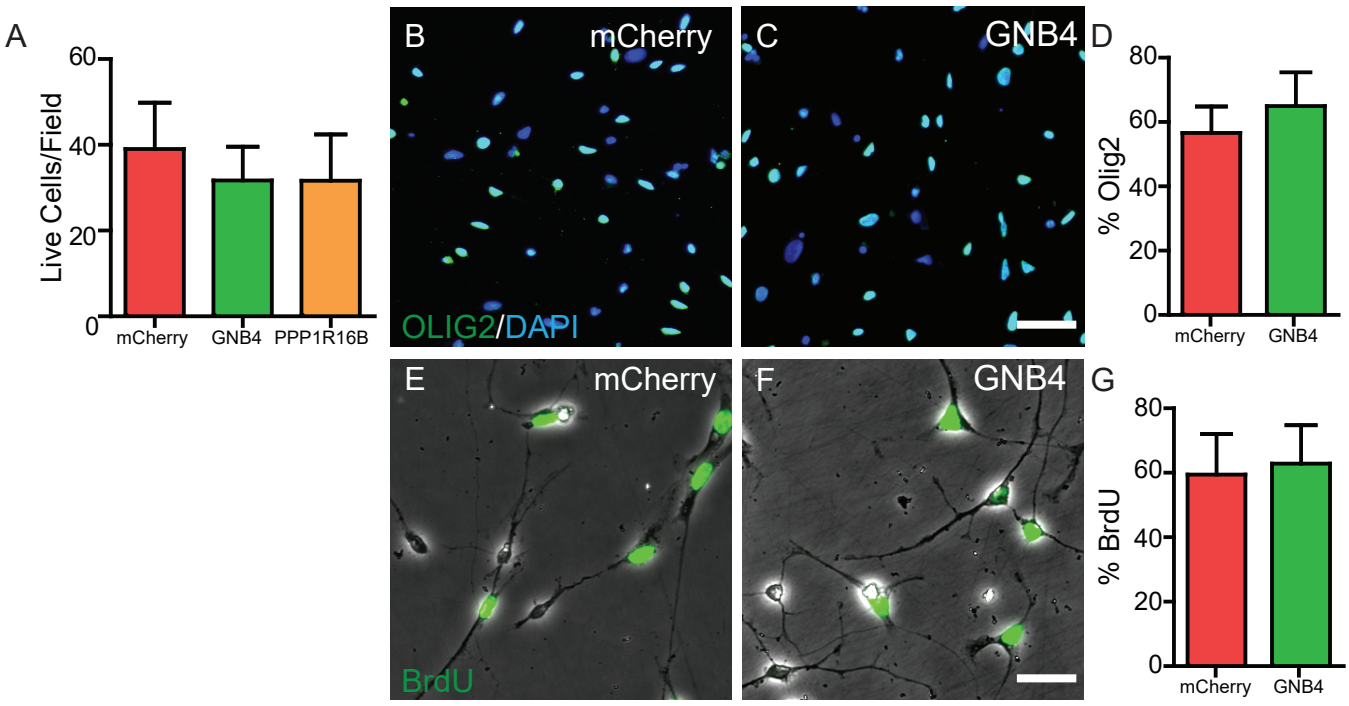
A
Live Cells/Field
60
40
20
0
mCherry
GNB4
PPP1R16B
B
mCherry
OLIG2/DAPI
C
GNB4
D
% Olig2
80
60
40
20
0
mCherry
GNB4
E
mCherry
BrdU
F
GNB4
G
% BrdU
80
60
40
20
0
mCherry
GNB4

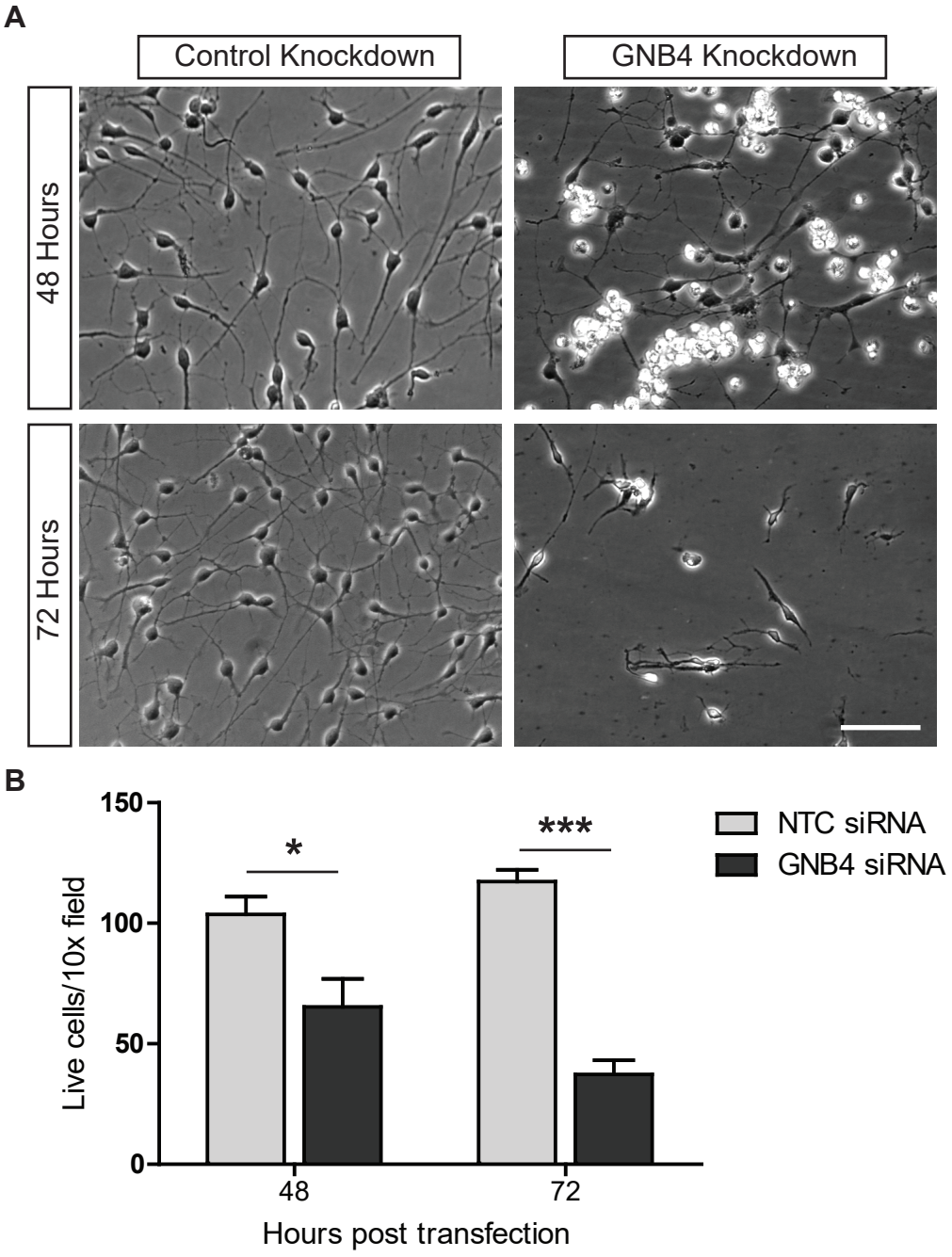
A
Control Knockdown
GNB4 Knockdown
48 Hours
72 Hours
B
150
100
50
0
Live cells/10x field
*
***
NTC siRNA
GNB4 siRNA
48
72
Hours post transfection

A

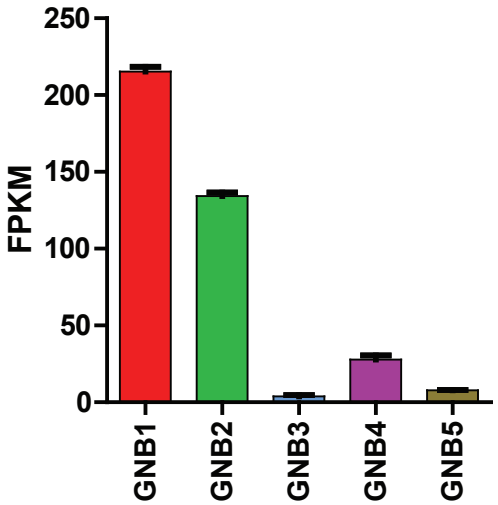

B

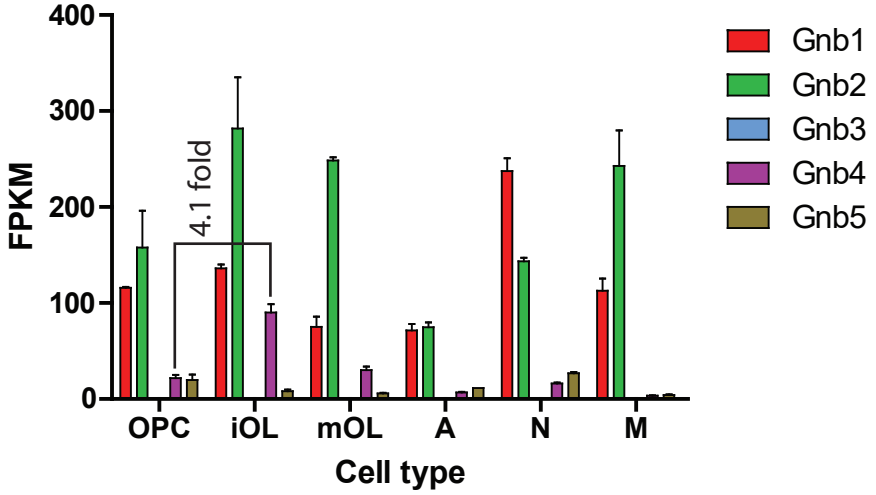

C

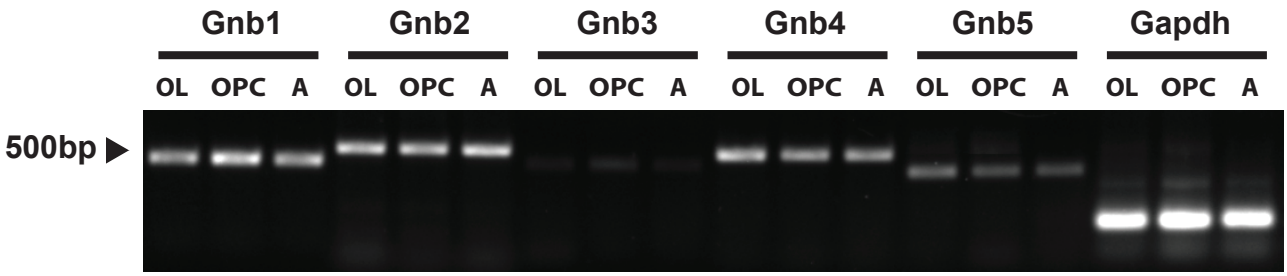

Gene	Forward	Reverse	Product Size(bp)
Gnb1	CTGGCAGGACATACAGGTTATC	TGAGTGCATCCCAGACATTAC	487
Gnb2	GGACAGCTACACCACTAACAA	TGTTGTCGTGGGAATACATGAG	560
Gnb3	CTCGGCTCACACAGGTTATC	CTTCAGAGAGTCCCAGACATTG	487
Gnb4	GGGATACGATTCCAGGCTACTA	ACCAGTGGCAAAGGCATATC	544
Gnb5	GCTTGTGGTGGTCTGGATAATA	ATCTGCCCTCAGGTCATAGA	453
Gapdh	GTGAAGGTCGGAGTGAACGG	CCTGGAAGATGGTGATGGGC	115

Figure S7

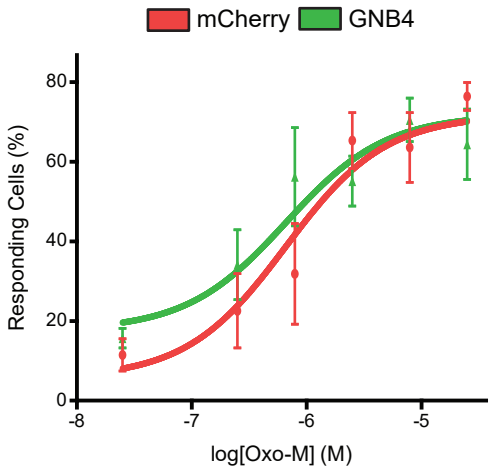

SUPPLEMENTAL FIGURE LEGENDS

Figure S1 (related to Figure 2). Summary of Weighted gene coexpression network analysis in cultured rat OPCs, isolated mouse cell populations, and PDGFRA/O4 sorted hOPCs.

For each data set:
A, fit of power-transformed gene-pairwise Pearson correlation with a scale free topology at each soft threshold. **B**, mean connectivity as a function of soft threshold. The power was set to 8 to transform the data to best fit with scale-free topology (marked in red). **C**, heatmap of Pearson correlations between unmerged module eigengenes. **D**, expression profiles of merged module eigengene. Merged modules were labeled according to the greatest overlap with modules identified in the profile of differentiating human OPCs (labeled with a 'D' suffix). **E**, correlation of module eigengenes with experimental parameters.

The power (soft threshold) was set to 8 (rat OPC; Dugas), 16 (mouse; Cahoy), 14 (hOPC; Abiraman).

Merged modules were labeled with a 'D', 'C', or 'A' suffix, for Dugas, Cahoy, and Abiraman datasets respectively.

Correlation with experimental parameters included:

Dugas: time and expression in $O4^+$ oligodendrocytes.

Cahoy: oligodendrocyte lineage and differentiation (i.e. up from $PDGF\alpha R^+$ OPC to MOG^+ OLG).

Abiraman: $PDGFRA^+$ OPC vs. $PDGFRA^-$ dissociate, $PDGFRA^+O4^+$ biased OPC vs. $PDGFRA^+O4^-$, and $PDGFRA^-O4^+$ immature oligodendrocyte (iOL) vs. $PDGFRA^+O4^+$ biased OPC

Figure S2 (related to Figure 5). Module eigengenes from four data sets. Heatmaps of every module eigengene expression in the four data sets. Rat (**B**), mouse (**C**) and sorted hOPC (**D**), modules are numbered per the WGCNA overlap analysis. If significant overlap was found, the matching module name is also provided.

Figure S3 (related to Figure 5). The effect of BCAS1 over-expression on human $PDGFRA^+$ OPCs. A, real-time quantitative PCR analysis of BCAS1 mRNA expression during human OPC differentiation (mean ± SEM $\log_2$ fold change relative to day 1 conditions, n=4 human samples). * and *** indicate posttest $p < 0.05$ and 0.001, respectively; Tukey's posttest vs. day 1 noGF conditions). **B-E**, hOPCs were infected with retroviruses expressing BCAS1 or an empty vector, and allowed to grow in the presence or absence of PDGF-AA (20 ng/ml) for 4 days. BrdU was pulsed 24 hours prior to fixation and cultures immunostained for O4 (**B**) and BrdU (**D**). Quantification and statistical analysis of O4 (**C**) and BrdU (**E**) proportions. As expected, growth media had a significant effect on $O4^+$ oligodendrocyte differentiation ($p<0.05$, significant effect of media conditions ($F=34.89$ [1,2]), 2-way ANOVA). BCAS1 virus did not affect the percentage of $O4^+$ cells ($p>0.05$, effect of virus ($F= 0.57$ [1,2], 2-way ANOVA). However, BCAS1 over-expression significantly reduced the proportion of dividing $BrdU^+$ hOPCs (2-way ANOVA, $F=25.2$ [1,2], $p=0.037$). Scale: 200 µm.

Figure S4 (related to Figure 5). GNB4 over-expression does not alter OPC proliferation or OLIG2 lineage status. hOPCs were infected with lentivirus overexpressing mCherry (Control) or GNB4 over-expressing virus, and allowed to differentiate for 4 days. Quantification after 4 days

showed no significant effect of GNB4 or PPP16R1B on live cell number (**A**), the proportion of Olig2$^+$ oligodendrocyte lineage cells (**B-D**), or the proportion of proliferative BrdU$^+$ cells (**E-G**) ($p > 0.05$, n = 4 fetal samples, unpaired t-test). Scale: 100µm (**B, C**), 50µm (**E, F**).

Figure S5 (related to Figure 5). GNB4 KD induces rapid hOPC death. hOPC were transfected with siRNAs targeting GNB4 or a scrambled control, and allowed to differentiate in the absence of mitogens (**A**). **Top**, Micrographs of hOPC in culture 48 hours after mitogen removal. GNB4 knockdown hOPC show reduced viability, observed as a reduction in cell number, rounded morphology, clumping of unviable cells. **Bottom**, Micrographs of hOPC following media change, 72 hours after mitogen removal. **B**, GNB4 knockdown hOPCs show substantially reduced cell number. *, *** indicate $p < 0.05$, 0.001, n = 3, two-way ANOVA with Bonferroni post-test. *Scale: 100µm.

Figure S6 (related to Figure 6). GNB subtype expression in OPCs. A, RNA-seq analysis of human OPCs indicates that GNB1/2 are more abundant in progenitors prior to differentiation. GNB3 was essentially not detected (mean ± SEM, n = 3 fetal human samples). **B**, RNA-seq analysis of mouse OPCs and OLGs (Zhang et al., 2014) indicates that GNB4 is strongly up-regulated during differentiation and becomes as abundant as GNB1/2 in immature oligodendrocytes, i.e., the equivalent stage to day 4 differentiating hOPCs (mean ± SEM, n = 2). **C**, RT-PCR analysis of G-protein β subunit expression in rat CG-4 OPCs (repeated three times, representative image shown). OPCs were either maintained in PDGF-AA/FGF conditions (OPC) or induced to differentiate into oligodendrocytes (OL) or astrocytes (A) prior to RNA extraction. RT-PCR revealed abundant expression of rat Gnb1/2/4 at all stages, whereas Gnb3/5 transcripts were not abundant, consistent with the mouse RNA-seq data. As such, $G_{\beta 4}$ is abundantly expressed by mouse, rat, and human immature oligodendrocytes. The primer sequences used are shown below the gel image.

Figure S7 (related to Figure 6). $G_{\beta 4}$ over-expression does not affect muscarinic activation. Fetal PDGFαR$^+$ hOPCs were cultured and infected with intracellular [Ca^{2+}] reporter GCaMP6s. Following infection with GNB4- or mCherry over-expression lentivirus, time-lapse microscopy of Ca^{2+} response after muscarinic agonist, Oxo-M, treatment was recorded and analyzed. The percentage of responding cells after Oxo-M addition is shown. GNB4 had no significant effect on EC_{50} for response to muscarinic stimulus ($LogEC_{50}$ = -5.9 ± 0.2 vs. -6.5 ± 0.3 for mCherry and GNB4, respectively, $p > 0.05$, n > 90 cells per condition from two individual human samples).

SUPPLEMENTAL TABLES

Table S1. See excel spreadsheet.

Table S2. See excel spreadsheet.

Table S3: Antibodies used.

Antibody	Host	Dilution	Source	Catalog Number
O4	Mouse IgM	1:25	Dr. James Goldman (Columbia University)	n/a
Olig2	Rabbit IgG	1:2000	Millipore Sigma	AB9610
Human Nuclei (hNA)	Mouse IgG1	1:100	Millipore Sigma	MAB1281
MBP	Rat	1:400	Abcam	AB7349
CC1	Mouse	1:50	EMD Chemicals	OP80
Ki67	Rabbit IgG	1:250	ThermoFisher Scientific	RM-9106-S1
GFAP	Mouse IgG1	1:800	BioLegend (Covance)	SMI-21R
BrdU	Rabbit IgG	1:1000	Bio-Rad AbD (Serotec Inc)	MCA2060

Table S4: Oligonucleotide primers for real-time quantitative PCR.

Gene	Primer Sequence (5' -> 3')	
hsGAPDH	Fwd:	GTGAAGGTCGGAGTCAACGG
	Rev:	CCTGGAAGATGGTGATGGGA
hsMBP	Fwd:	GGCAGAGCGTCCGACTATAAA
	Rev:	CGACTATCTCTTCCTCCCAGCTT
hsCSPG4	Fwd:	GAGGACAGCTGGAGCTCTAGGGT
	Rev:	AGGCCTGGGACCAAAGCGGA
hsBCAS1	Fwd:	AGGCCTGGGACCAAAGCGGA
	Rev:	ACCTGGTGGGAACCGTGCTGA
hsGNB4	Fwd:	AAGTGGGCGTCTCTTGTTGGC
	Rev:	CCAGCAAGGACACCTGCACGAT
hsPPP1R16B	Fwd:	AGGACCCTAACCCCAGGCTGG
	Rev:	GGAGCCCGGAGGCCATTCTC

SUPPLEMENTAL EXPERIMENTAL PROCEDURES

Cell and Tissue Samples

Fetal brain samples (18-22 wk gestational age) were obtained from patients who consented to tissue use under protocols approved by the State University of New York at Buffalo Institutional Review Board. Cortical tissue, including ventricular and subventricular zones, was dissociated and prepared as previously described (Windrem et al., 2002) and cultured in serum-free media with 10 ng/ml FGF2 (PeproTech, Inc., Rocky Hill, NY, USA) (as detailed in Sim et al., 2011).

Magnetic isolation of human PDGFRA$^+$ OPCs

Magnetic sorting of PDGFRA was performed as described (Sim et al., 2011). Briefly, cells were recovered and stained with PDGFRA PE-conjugated purified mouse $IgG2_a$ antibody (BD Pharmingen, San Diego, CA). Cells were washed and rat anti-mouse IgG_{2a+b} secondary antibody was added according to the manufacturer's instructions (Miltenyi Biotech, Auburn, CA). Magnetic sorting was performed using LS column selection and a sample of positive cells collected for subsequent flow cytometry-based analysis of purity.

Immunocytochemistry

Cultures were exposed continuously to 10 µg/ml BrdU beginning 24 hours before fixation. O4 supernatant (gift of Dr. James Goldman, Columbia University) was applied to live cultures for 30 minutes at 37ºC (1:25 dilution) pre-fixation. Cultures were washed and fixed in 4% paraformaldehyde and immunostained for OLIG2 (1:2000, Millipore, Billerica, MA) or BrdU (1:1000, Serotec, Raleigh, NC). Secondary antibodies, Alexa-488, -647 conjugated goat anti-rabbit IgG, mouse IgM or rat IgG antibodies were used at a dilution of 1:500 (Invitrogen, Carlsbad, CA). The number of O4, OLIG2 and BrdU stained and unstained cells were quantified in 10 random fields, representative of over 250 random cells.

Real-time RT-PCR analyses

PDGFRA$^+$ hOPCs were plated onto 35 mm tissue culture plates coated with poly-L-ornithine and laminin at 1×10^5 cells/ml in serum-free media as described above. mRNA was isolated using an E.Z.N.A Total RNA Kit I (Omega Bio-Tek, Norcross, GA) according to manufacturer's protocols and cDNA prepared (SuperScript III Kit; Invitrogen, Carlsbad, CA). Human-specific primers for SYBR green-based PCR were designed using Primer Express (v1, Applied Biosystems, Foster City, CA) (**Table S4**). Samples were run in duplicates for real-time PCR (MyiQ; Bio-Rad, Hercules, CA), and gene expression calculated by $\Delta\Delta C_t$ analysis using the primer efficiency, as previously described (Pfaffl, 2004). Gene expression was normalized to the control gene GAPDH. Statistical significance was tested on $\log_2$-transformed data using repeated measures 1-way ANOVA followed by Tukey's posttest (GraphPad Prism version 5.01 software).

Microarray analysis

Prior to array analysis, mRNA was amplified using NuGEN WT-Ovation Pico RNA amplification system according to manufacturer's instructions. Amplified product was hybridized onto Illumina HT-12v3 bead arrays according to manufacturer's instructions (Illumina). All microarray data were analyzed using R/Bioconductor (Gentleman et al., 2004). The complete analysis code is available on request (fjsim@buffalo.edu). The complete microarray data are available at NCBI GEO GSE36431 and may be directly browsed via FINDdb (www.FindDB.org). Briefly, raw data were loaded using the *lumi* package (Du et al., 2008), samples were background corrected, vsn transformed/normalized, and poor quality data were filtered using a detection call p-value cutoff of 0.01. Exploratory analysis was then performed using 3dPCA and hierarchical clustering - *analysisPipeline* package, Sim et al. (2011). A custom annotation package (*nuID.combined.db*) was developed to improve annotation. This package combined annotations

from Agilent, Ensembl (Durinck et al., 2005), and *lumiHumanAll.db* (Du et al., 2008). The expression of genes associated with OPC fate and oligodendrocyte differentiation were visualized following normalization to day zero median expression (heatmap.2, *gplots*).

For cross-species analysis, we compiled raw data from various published data sets. The expression profiles of freshly isolated PDGFRA and O4 FACS-isolated hOPC cells was pre-processed exactly as described above (Abiraman et al., 2015). The profiles of differentiating rat $A2B5^+$ OPC data (GSE9566) (Dugas et al., 2006) and freshly isolated mouse cells, including OPCs (GSE9566) (Cahoy et al., 2008) were normalized by justRMA (*Affy*) and non-informative probe sets filtered (*farms*) (Hochreiter et al., 2006). Affymetrix microarray data were annotated using Bioconductor packages *rgu34abc* and *mouse4302*, and gene expression data matrices were generated using nsFilter (*genefilter*).

Weighted gene coexpression network analysis (WGCNA)

WGCNA was performed using the R/Bioconductor package (Langfelder and Horvath, 2008) following the method described in Konopka et al. (2009). A total of 12,494 genes were included in the hOPC differentiation analysis. Similar analyses were performed with PDGFRA/O4 hOPCs (12,404 genes), mouse cell-type specific (11,202 genes), and rat OPC differentiation (11,091 genes) data. Module membership was defined as the intramodular connectivity representing the sum of Pearson correlations to each gene in the module. Characterization of module function was first performed by analysis of the module eigengene which is defined as the first principle component of the expression profiles of its constitutive genes. The expression profile of each module eigengene was correlated with experimental parameters specific to each data set. For example, we correlated the hOPC differentiation data module eigengenes with both time *in vitro* and media conditions to identify modules whose expression was up-regulated in differentiating conditions.

The degree of species conservation between WGCNA-derived modules was analyzed by hypergeometric analysis of module overlap, as described in Oldham et al. (2008). Briefly, human Entrez ID homologs of rat and mouse genes were found in each data set using a combination of NCBI homologene, ensembl homologs found using *biomaRt*, and Bioconductor homology packages - *analysisPipeline* package (Sim et al., 2011). Significance was calculated using a one-sided hypergeometric test of overlapping genes in each module (using the top 50^{th} percentile of connected genes in each module), and corrected for multiple comparisons by false discovery rate (q-value < 0.1). Modules from different networks with significant overlap were assigned the same number, with the suffix denoting the dataset [e.g. M15 for hOPC differentiation, M15D for Dugas et al. (2006), M15C for Cahoy et al. (2008), and M15A for Abiraman et al. (2015)]. If a module overlapped with more than one module from the hOPC differentiation dataset, we assigned the module number based on the lowest p-value.

Over-representation of specific gene ontology terms was performed using *topGO* (Alexa et al., 2006). Module hub genes were defined as the top 30 genes with highest intramodule connectivity, i.e. the sum of the Pearson correlation to all other module members. These were visualized as a graph using *Rgraphviz.*

Viral cloning and packaging

Retroviral BCAS1-IRES-GFP and control MIG-GFP virus were used at 2 multiplicity of infection (MOI) (gift of Dr. Magdalena A. Petryniak, Oregon Health & Science University). To generate lentiviral over-expression vectors, the coding region of each gene was PCR-amplified from fetal human brain cDNA and cloned into a lentiviral expression plasmid as described previously (Wang et al., 2014) (pTRIP-EF1α; gift from Abdel Benraiss, University of Rochester, Rochester, NY). Virus was prepared by $CaPO_4$-based transfection as described in Jordan et al. (1996). Collected virus was then concentrated using high-speed centrifugation (50,000 g, 90 min; Beckman Coulter Rotor JA-25.5). Viral titers were measured using real-time RT-PCR for

expression of WPRE (Geraerts et al., 2006) and compared to titers determined using flow cytometry with TRIP-mCherry virus. hOPCs were infected one day after seeding at one MOI and the infection was stopped at 24 hours by exchange of culture medium.

siRNA-mediated gene knockdown

siRNA molecules were obtained from ThermoFisher Scientific, three targeting GNB4 (HSS126985, HSS126987, HSS184233), and a scrambled negative control (#12935112). hOPCs were seeded as previously described at a density of 10^5 cells/ml onto 48-well plates. 24 hours later, siRNA were transfected, combined or individually, at a total concentration of 100μM siRNA, using Lipofectamine RNAiMAX transfection reagent (ThermoFisher Scientific). Knockdown efficiency was determined by qPCR, 48 hours post-transfection.

Cloning of LV-EF1a:GCaMP6s

We PCR/TOPO cloned the coding region of GCaMP6s from pLP-CMV-GCaMP6s-CAAX (AddGene, #52228)(Tsai et al., 2014) into pCR2.1 TOPO4 plasmid (Invitrogen). The GCaMP6s fragment was then subcloned using unique 5' SpeI and 3' PspXI restriction sites into lentiviral pTRIP-EF1a (derived from pTRIP-EF1a, in Sevin et al., 2006) (gift of Abdel Benraiss, University of Rochester). Lentiviruses were prepared as described above. Viruses were tittered on the basis of matched mCherry-expressing virus using flow cytometry for mCherry fluorescence and directly compared to GCaMP6s virus using real-time quantitative PCR for the WPRE sequence (Geraerts et al., 2006). GCaMP6s expression was confirmed using CHO-M_3R expressing cells (gift of Dr. Jurgen Wess) by fluorescence imaging following addition of carbachol or $CaCl_2$. For all imaging experiments, hOPCs were infected at one MOI for 24 hours followed by complete media replacement. One hour prior to imaging, media was replaced with phenol red-free media.

Calcium imaging using LV-EF1a:GCaMP6s

All calcium imaging experiments were performed at 10x magnification using an Olympus IX51 with a Prior XYZ stage equipped with a Hamamatsu ORCA-ER camera using a 1x TV lens. All phase images and fluorescent time-lapse acquisitions were performed at room temperature and captured using μManager (Edelstein et al., 2010a). Oxotremorine-M (Tocris) was thawed immediately prior to each experiment. Two fields per preparation were imaged for each condition, at 2-second intervals for 10-12 minutes. Drug addition occurred 1 min after the start of imaging. Phase images were used to generate regions of interest corresponding to the soma of every cell by thresholding and supervised analysis. Rolling ball subtraction was performed on fluorescence image frames, and the mean pixel intensity was calculated for each cell using ImageJ. Baseline cellular GCaMP6s fluorescence was determined immediately prior to drug addition on a per cell basis. Analysis of calcium wave characteristics, such as amplitude, peak number, frequency, and subsequent statistics were performed in R (complete analysis code is available on request). Briefly, calcium response curves were loess fitted (*zoo*) (Zeileis and Grothendieck, 2005), and the local minima and maxima were calculated. A local maximum was considered a peak if its amplitude increased > 35% from its local minimum. Response duration was measured from the onset of the first peak to the end of the last peak. The area under the curve was calculated for the duration of the response. The relationship between dose and the percentage of responding cells was fitted to the following Hill equation: $y = \frac{Top - Bottom}{1+(10)^{(EC_{50}-x)}}$. For each parameter, a linear model was used for two-way ANOVA with Tukey HSD analysis, fitted using virus (mCherry or GNB4), oxotremorine dose, and the interaction of these variables as predictors, as well as the source human sample to consider individual tissue sample variability.

Luciferase Reporter Pathway Analysis

PDGFRA$^+$ hOPCs from two patient sources were mixed 1:1 and plated in 96-well tissue culture plates coated with poly-L-ornithine and laminin at 2.5×10^4 cells/ml in serum-free media as

described above. 24 hours after seeding, cells were transduced (10 MOI) with Cignal Lenti Luciferase Reporter (Qiagen) for PKC/Ca^{2+} (NFAT, CLS-015L), MAPK/ERK (Elk/SRF, CLS-010L), MAPK/JNK (AP1, CLS-011L), cAMP/PKA (CREB, CLS-002L) or a negative control (CLS-NCL). 24 hours after initial infection, hOPCs were infected with mCherry or GNB4-overexpressing lentivirus (1 MOI). Luminescence responses were quantified 60 hours later using a Promega Bright-Glo reagent in a Bio-Tek plate reader, in accordance with the manufacturer's protocols. Luminescence responses were normalized to the negative control response. The measurements are presented as mean ± SEM for three replicates of two human sample sources.

Transplantation into shiverer/rag2 mice

Animals and surgery. All experiments using *shiverer/rag2* mice (a gift of Dr. Steven A. Goldman, University of Rochester) (Windrem et al., 2008) were performed according to protocols approved by the University at Buffalo Institutional Animal Care and Use Committee (IACUC). If necessary, newborn pups were genotyped on the day of birth to identify homozygote shiverer mice. hOPCs were cultured for up to 1 week in serum-free media (SFM) containing PDGF-AA/FGF and frozen using ProFreeze (Lonza) prior to surgery. Cells were thawed and then infected 24 hrs later with lentivirus (1 MOI) and allowed to recover for 1-2 days prior to transplantation. Cells were prepared for injection by re-suspending cells in HBSS(-) at 1×10^5 cells per µl. Injections were performed as previously described (Sim et al., 2011). Briefly, pups were anesthetized using hypothermia and 5×10^4 cells were injected bilaterally into the corpus callosa of postnatal day 2-3 pups. Cells were injected through pulled glass pipettes, inserted directly through the skull. Animals were sacrificed and perfused with saline followed by 4% paraformaldehyde after 8 weeks.

In vivo immunostaining. Cryopreserved coronal sections of mouse forebrain (16 µm) were cut and brains were sampled every 160 µm. Immunohistochemistry was performed as described (Sim et al., 2011). Human cells were identified with mouse anti-human nuclei antibody (hNA; 1:100, clone 235-1; Millipore), and sections were stained for MBP (1:400; Abcam, Inc., Cambridge, UK), CC1 (1:50; Millipore), human GFAP (1:800; Covance, Inc., Princeton, NJ, USA), and Ki67 (1:250, Clone SP6, Thermo Scientific). Alexa Fluor-conjugated secondary antibodies (Invitrogen) were used at 1:500.

Microscopy. Images were captured at 20× with a motorized fluorescence microscope (Olympus IX-51) using µManager (Edelstein et al., 2010b), and subsequent analyses performed with Fiji (Schindelin et al., 2012). 4-5 sections every 160 µm were sampled from highly engrafted regions in the corpus callosum. Quantification of hNA^+ cell density and phenotype was performed by counting cells in midline and lateral regions in the corpus callosum and more than 1,000 cells were counted per animal. hNA^+ cells were counted using the ITCN plugin (Byun et al., 2006). The proportion of hNA^+ cells expressing CC1, Ki67, and GFAP was determined by manual counting with between 500 and 1,000 cells counted per animal. Confocal microscopy was performed using a Zeiss LSM510 Meta Confocal and analysis was performed in Fiji software. As described previously (Wang et al., 2014), a stack of 40 optical sections was obtained every 0.1 µm, and the number of myelinated fibers that crossed three perpendicular sampling lines, placed randomly across the image, were counted.

SUPPLEMENTAL REFERENCES

Abiraman, K., Pol, S.U., O'Bara, M.A., Chen, G.D., Khaku, Z.M., Wang, J., Thorn, D., Vedia, B.H., Ekwegbalu, E.C., Li, J.X.*, et al.* (2015). Anti-muscarinic adjunct therapy accelerates functional human oligodendrocyte repair. J Neurosci *35*, 3676-3688.

Alexa, A., Rahnenfuhrer, J., and Lengauer, T. (2006). Improved scoring of functional groups from gene expression data by decorrelating GO graph structure. Bioinformatics *22*, 1600-1607.

Byun, J., Verardo, M.R., Sumengen, B., Lewis, G.P., Manjunath, B.S., and Fisher, S.K. (2006). Automated tool for the detection of cell nuclei in digital microscopic images: application to retinal images. Molecular vision *12*, 949-960.

Cahoy, J.D., Emery, B., Kaushal, A., Foo, L.C., Zamanian, J.L., Christopherson, K.S., Xing, Y., Lubischer, J.L., Krieg, P.A., Krupenko, S.A.*, et al.* (2008). A transcriptome database for astrocytes, neurons, and oligodendrocytes: a new resource for understanding brain development and function. J Neurosci *28*, 264-278.

Du, P., Kibbe, W.A., and Lin, S.M. (2008). lumi: a pipeline for processing Illumina microarray. Bioinformatics *24*, 1547-1548.

Dugas, J.C., Tai, Y.C., Speed, T.P., Ngai, J., and Barres, B.A. (2006). Functional genomic analysis of oligodendrocyte differentiation. J Neurosci *26*, 10967-10983.

Durinck, S., Moreau, Y., Kasprzyk, A., Davis, S., De Moor, B., Brazma, A., and Huber, W. (2005). BioMart and Bioconductor: a powerful link between biological databases and microarray data analysis. Bioinformatics *21*, 3439-3440.

Edelstein, A., Amodaj, N., Hoover, K., Vale, R., and Stuurman, N. (2010a). Computer control of microscopes using microManager. Curr Protoc Mol Biol *Chapter 14*, Unit14.20.

Edelstein, A., Amodaj, N., Hoover, K., Vale, R., and Stuurman, N. (2010b). Computer control of microscopes using microManager. Curr Protoc Mol Biol *Chapter 14*, Unit14 20.

Gentleman, R.C., Carey, V.J., Bates, D.M., Bolstad, B., Dettling, M., Dudoit, S., Ellis, B., Gautier, L., Ge, Y., Gentry, J.*, et al.* (2004). Bioconductor: open software development for computational biology and bioinformatics. Genome Biol *5*, R80.

Geraerts, M., Willems, S., Baekelandt, V., Debyser, Z., and Gijsbers, R. (2006). Comparison of lentiviral vector titration methods. BMC biotechnology *6*, 34.

Hochreiter, S., Clevert, D.A., and Obermayer, K. (2006). A new summarization method for Affymetrix probe level data. Bioinformatics *22*, 943-949.

Jordan, M., Schallhorn, A., and Wurm, F.M. (1996). Transfecting mammalian cells: optimization of critical parameters affecting calcium-phosphate precipitate formation. Nucleic acids research *24*, 596-601.

Konopka, G., Bomar, J.M., Winden, K., Coppola, G., Jonsson, Z.O., Gao, F., Peng, S., Preuss, T.M., Wohlschlegel, J.A., and Geschwind, D.H. (2009). Human-specific transcriptional regulation of CNS development genes by FOXP2. Nature *462*, 213-217.

Langfelder, P., and Horvath, S. (2008). WGCNA: an R package for weighted correlation network analysis. BMC Bioinformatics *9*, 559.

Oldham, M.C., Konopka, G., Iwamoto, K., Langfelder, P., Kato, T., Horvath, S., and Geschwind, D.H. (2008). Functional organization of the transcriptome in human brain. Nat Neurosci *11*, 1271-1282.

Pfaffl, M.W. (2004). Quantification strategies in real time-PCR. In A-Z of Quantitative PCR, S.A. Bustin, ed. (La Jolla, CA: International University Line), pp. 87-112.

Schindelin, J., Arganda-Carreras, I., Frise, E., Kaynig, V., Longair, M., Pietzsch, T., Preibisch, S., Rueden, C., Saalfeld, S., Schmid, B.*, et al.* (2012). Fiji: an open-source platform for biological-image analysis. Nature methods *9*, 676-682.

Sevin, C., Benraiss, A., Van Dam, D., Bonnin, D., Nagels, G., Verot, L., Laurendeau, I., Vidaud, M., Gieselmann, V., Vanier, M.*, et al.* (2006). Intracerebral adeno-associated virus-mediated gene

transfer in rapidly progressive forms of metachromatic leukodystrophy. Hum Mol Genet *15*, 53-64.
Sim, F.J., McClain, C.R., Schanz, S.J., Protack, T.L., Windrem, M.S., and Goldman, S.A. (2011). CD140a identifies a population of highly myelinogenic, migration-competent and efficiently engrafting human oligodendrocyte progenitor cells. Nature biotechnology *29*, 934-941.
Tsai, F.C., Seki, A., Yang, H.W., Hayer, A., Carrasco, S., Malmersjo, S., and Meyer, T. (2014). A polarized Ca2+, diacylglycerol and STIM1 signalling system regulates directed cell migration. Nat Cell Biol *16*, 133-144.
Wang, J., Pol, S.U., Haberman, A.K., Wang, C., O'Bara, M.A., and Sim, F.J. (2014). Transcription factor induction of human oligodendrocyte progenitor fate and differentiation. Proc Natl Acad Sci U S A *111*, E2885-2894.
Windrem, M.S., Roy, N.S., Wang, J., Nunes, M., Benraiss, A., Goodman, R., McKhann, G.M., 2nd, and Goldman, S.A. (2002). Progenitor cells derived from the adult human subcortical white matter disperse and differentiate as oligodendrocytes within demyelinated lesions of the rat brain. Journal of neuroscience research *69*, 966-975.
Windrem, M.S., Schanz, S.J., Guo, M., Tian, G.F., Washco, V., Stanwood, N., Rasband, M., Roy, N.S., Nedergaard, M., Havton, L.A.*, et al.* (2008). Neonatal chimerization with human glial progenitor cells can both remyelinate and rescue the otherwise lethally hypomyelinated shiverer mouse. Cell stem cell *2*, 553-565.
Zeileis, A., and Grothendieck, G. (2005). zoo: S3 Infrastructure for Regular and Irregular Time Series. Journal of Statistical Software; Vol 1, Issue 6 (2005).
Zhang, Y., Chen, K., Sloan, S.A., Bennett, M.L., Scholze, A.R., O'Keeffe, S., Phatnani, H.P., Guarnieri, P., Caneda, C., Ruderisch, N.*, et al.* (2014). An RNA-sequencing transcriptome and splicing database of glia, neurons, and vascular cells of the cerebral cortex. J Neurosci *34*, 11929-11947.